

A Permian large igneous province in Tarim and Central Asian orogenic belt, NW China: Results of a ca. 275 Ma mantle plume?

Chuan-Lin Zhang^{1,2,†}, Zheng-Xiang Li³, Xian-Hua Li⁴, Yi-Gang Xu¹, Gang Zhou⁵, and Hai-Min Ye^{2,4}

¹Key Laboratory of Isotope Geochronology and Geochemistry, Guangzhou Institute of Geochemistry, Chinese Academy of Sciences, Guangzhou 510640, China

²Nanjing Institute of Geology and Mineral Resources, Nanjing 210016, China

³Institute for Geoscience Research, Department of Applied Geology, Curtin University of Technology, GPO Box U1987, Perth, WA 6845, Australia

⁴State Key Laboratory of Lithospheric Evolution, Institute of Geology and Geophysics, Chinese Academy of Sciences, Beijing 100029, China

⁵Xinjiang Bureau of Geology and Mineral Resources, Altay 836500, China

ABSTRACT

New sensitive high-resolution ion microprobe (SHRIMP) U-Pb zircon ages, geochemical data, and a synthesis of existing stratigraphic, geochronologic, and geochemical results from the Tarim block and the Central Asian orogenic belt in northwestern China suggest the presence of a Permian (ca. 275 Ma) large igneous province (the Bachu large igneous province). The large igneous province consists predominantly of coeval mafic rocks (basalts and mafic-ultramafic intrusions) having an aerial coverage of more than 600,000 km², and its formation was accompanied by voluminous emplacement of A-type granites. This large igneous province, interpreted to be of mantle plume origin, is ~15 m.y. older than the ca. 260 Ma Emeishan large igneous province in southwestern China and ~25 m.y. older than the 251 Ma Siberian Trap in Russia. Such a sudden flair up of plume activity in the Permian may represent the early stage of the Pangean superplume event. The Permian plumes likely played a role in late Paleozoic rapid continental crustal growth in the Central Asian orogenic belt. In addition, there appear to be two types of mantle geochemical provinces (domains) in the region, a long-term enriched Tarim province and a subduction-metasomatized and depleted Central Asian orogenic belt province.

INTRODUCTION

The western part of the Central Asian orogenic belt in the Xinjiang Uygur Autonomous Region, northwestern China (Fig. 1), is believed

to have been consolidated by the mid-Carboniferous (Sengör et al., 1993; Zhou et al., 2004; Li, 2006; Zhao et al., 2007; Yuan et al., 2007). The Tarim block in southern Xinjiang is also believed by some to have been amalgamated with the Central Asian orogenic belt by that time (Xinjiang B.G.M.R., 1993; Shu et al., 2000; Li, 2006), though Zhang et al. (2007) recently suggested that orogenesis in the Xinjiang section of the Central Asian orogenic belt continued until the Triassic, based on geochronological data from eclogites in Western Tianshan. Nonetheless, because (1) the ages of the ophiolites in southern Altay and Tianshan range from 540 Ma to 325 Ma, and no ophiolite younger than 320 Ma has ever been documented, and (2) late Carboniferous to Permian granites are typically of postorogenic type (Han et al., 1999, 2004, 2006; Jiang et al., 2001; Chen and Jahn, 2004), it is likely that the Tarim block and the western part of the Central Asian orogenic belt were amalgamated by ca. 320 Ma.

The western Central Asian orogenic belt is renowned for being an area of major continental crustal growth in the late Paleozoic, as shown by an enormous amount of Permian-Carboniferous juvenile magmatism in the region (e.g., Jahn et al., 2004). However, the cause(s) of such an episode of crustal growth is still poorly understood. Magmatic products include Permian basalts, mafic-ultramafic intrusions, and A-type granites that are widespread in the Tarim block, the Tianshan Ranges, the Altay Mountains, and several basins north of Tianshan (the Santanghu, Tuha, and Junggar Basins; Fig. 1). Published tectonic settings for these coeval igneous rocks include melting due to postorogenic slab delamination (a predominant view; e.g., Han et al., 1999; Solomovich and Trifonov, 2002; Jahn et al., 2004; Chen and Jahn, 2004; D.W. Zhou

et al., 2006; X.H. Zhang et al., 2008), continental rifting magmatism due to the north-dipping subduction of the Paleotethys oceanic crust (Yang et al., 1995, 2007), magmatism in an extensional-transensional tectonic regime (DeJong et al., 2008), and mantle-plume-related processes (Zhou et al., 2004; Xia et al., 2004; Borisenko et al., 2006; C.L. Zhang et al., 2008; Pirajno et al., 2008; Yarmolyuk and Kozlovsky, 2009).

In order to further test these competing models, we obtained new sensitive high-resolution ion microprobe (SHRIMP) U-Pb zircon geochronological and geochemical data for mafic and granitic intrusions south of Altay City, and conducted a comprehensive review of existing stratigraphic, geochronologic, and geochemical results from the Xinjiang region, covering a lateral extent of ~1500 km. Based on these data, we argue that a Permian mantle plume in Tarim and the western Central Asian orogenic belt could account for the formation of the voluminous basalts, ultramafic-mafic intrusions, and A-type granites, and that this Permian plume event contributed to the late Paleozoic continental growth in the western Central Asian orogenic belt.

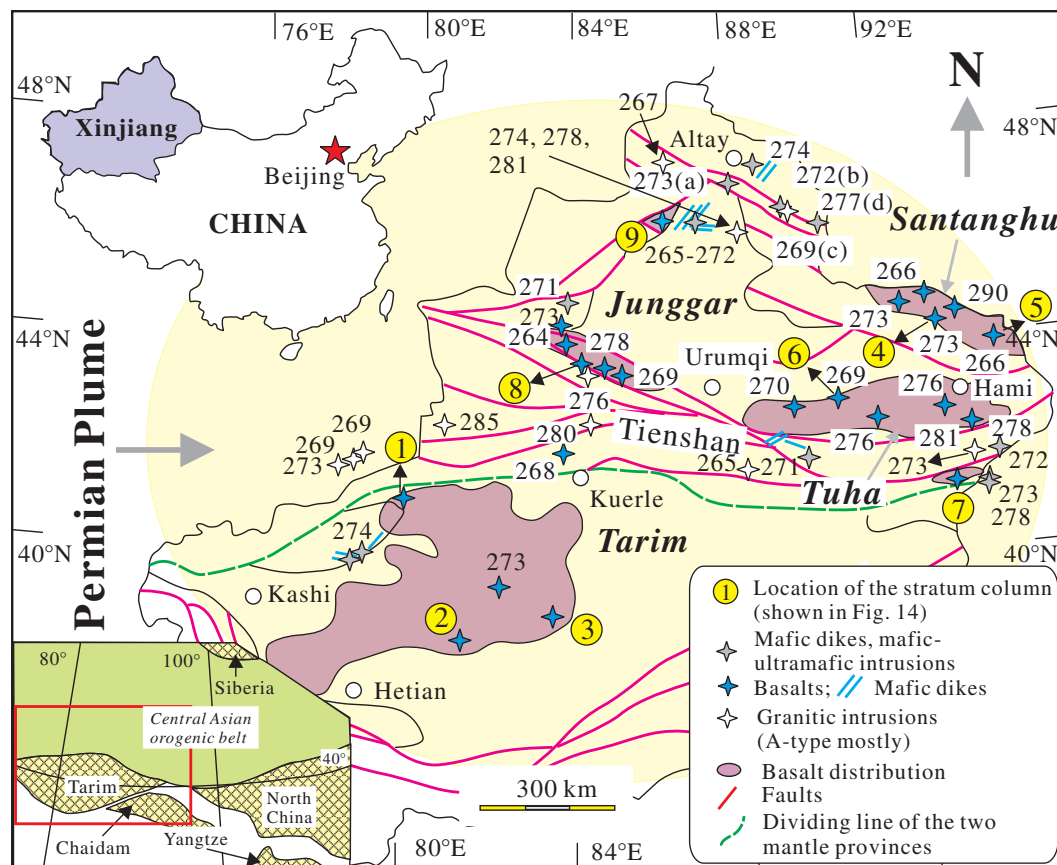
PERMIAN INTRUSIVE ROCKS SOUTH OF ALTAY

Regional Geology and Petrography

We investigated intrusive rocks in the southern part of the Altay orogenic belt at the western part of the Central Asian orogenic belt (Figs. 1 and 2A). The Altay orogenic belt is considered to have been consolidated with the Junggar block at ca. 380–360 Ma along the Erqisi (west)–Mayinebo (east) suture zone (Yuan et al., 2007; Tang et al., 2007; Sun et al., 2008). This is supported by the formation of the late

[†]E-mail: zchuanlin@yahoo.com.cn

Figure 1. Sketch map of geologic tectonic units of the Tarim block and part of the Central Asian orogenic belt (CAOB) in Xinjiang, showing the distribution of the Permian basalts, ultramafic-mafic intrusions, mafic dikes, and A-type granites, and their ages (the red, blue, and yellow stars represent the locations of the reported ages of the mafic dikes and mafic-ultramafic intrusions, basalts, and granitic intrusions, respectively). Ages obtained in this study are marked with a, b, c, and d (data and U-Pb concordia plots are presented in Table 1 and Figure 3). Inset in the lower-left corner shows the locations of the Central Asian orogenic belt and the major continental blocks in the study region.



Carboniferous to Permian anorogenic granites and the continental facies of the Permian strata (Xinjiang B.G.M.R., 1999; Zhou et al., 2009). Our study focuses on four types of Permian intrusive rocks in the region south of Altay, i.e., the Hongguleneng ultramafic complex, the Mayinebo gabbro, the Dasazi bimodal intrusive complex, and the Chaergan granites (annotated with a, b, c, and d in Figs. 1 and 2).

Hongguleneng Ultramafic Intrusions

Previous studies have suggested that the Hongguleneng ultramafic-mafic rocks were members of a late Neoproterozoic to early Paleozoic ophiolite complex between the Altay orogenic belt and the Junggar block (Fig. 2A; Bai and Zhou, 1988, 1989, 1991; Peng et al., 1991; Huang et al., 1999). A Sm-Nd isochron age of 626 ± 25 Ma was reported by Huang et al. (1999). Main rock types of the complex include serpentinized dunite, lherzolite, pyroxenite, websterite, and gabbro. All the rocks are cumulates, containing variable olivine, orthopyroxene, clinopyroxene, plagioclase, and spinel, and they constitute a layered intrusive complex (for detailed petrographic descriptions, see Bai and Zhou, 1989; Peng et al., 1991). The ultramafic members are intensively serpentinized, but relic olivine and pyroxene are well preserved in thin sections. On several outcrops,

gabbroic pegmatite with megacrystal pyroxene and plagioclase can be seen. All these features suggest that the complex was crystallized from a basaltic magma.

Mayinebo Gabbroic Stocks and Dikes

The Mayinebo gabbroic stocks and dikes intrude mainly the ca. 289 Ma Mayinebo granites and the Sinian Kuwei Group (G. Zhou et al., 2006; Fig. 2B). They are fine grained, and no accumulation textures are observed in thin sections. Main minerals are pyroxene (50%–70%, clinopyroxene + orthopyroxene), plagioclase (30%–50%), and minor olivine and Ti-Fe oxides. In the central part of one stock (with ~ 0.1 km² of exposure), there are gradual transitions between fine-grained gabbro and coarse-grained gabbro (or gabbroic pegmatite). A coarse-grained gabbroic sample, consisting of $\sim 50\%$ plagioclase, $\sim 45\%$ clinopyroxene, and $\sim 5\%$ quartz, was collected for geochronological analyses (Fig. 2B; sample 07AL03, corresponding to the geochemical sample 07AL03–11).

Dasazi Gabbro-Granodiorite Bimodal Intrusive Complex

In the Dasazi gabbro-granodiorite (granite) complex (Fig. 2C), gabbro and granodiorite are found to be interweaving at the outcrop scale,

and at several outcrops, gabbros are seen to have been gradually “dissolved” into the granodiorites. These features indicate that gabbro and granodiorite were emplaced at the same time, with possible mass exchanges between them. The gabbro is mainly composed of plagioclase (40%–50%), clinopyroxene (40%–50%), and minor hornblende (1%–10%), biotite (<2%), and quartz (<1%). Accessory minerals include Ti-Fe oxides, apatite, and zircon. The granodiorite is mainly composed of plagioclase (30%–45%), microcline (15%–25%), quartz (25%–35%), hornblende (5%–20%), biotite (1%–5%), and accessory minerals such as apatite and zircon. All the rock types are fresh, and no deformation or hydrothermal alteration has been observed in the field. A 275 ± 12 Ma whole-rock Rb-Sr isochron age was obtained by the No. 2 Geological Party of Xinjiang Bureau of Geology and Mineral Resources (1998).

Chaergan Granite

The Chaergan granite is located northeast of the Mayinebo fault (Fig. 2D). It intrudes the Sinian Kuwei Group. Main rock types include granite, granodiorite, and potassic granite. Gabbro enclaves with 0.5–2 m \times 0.5–2 m dimensions are seen mingling with the granite at several outcrops. The granitic rocks are composed

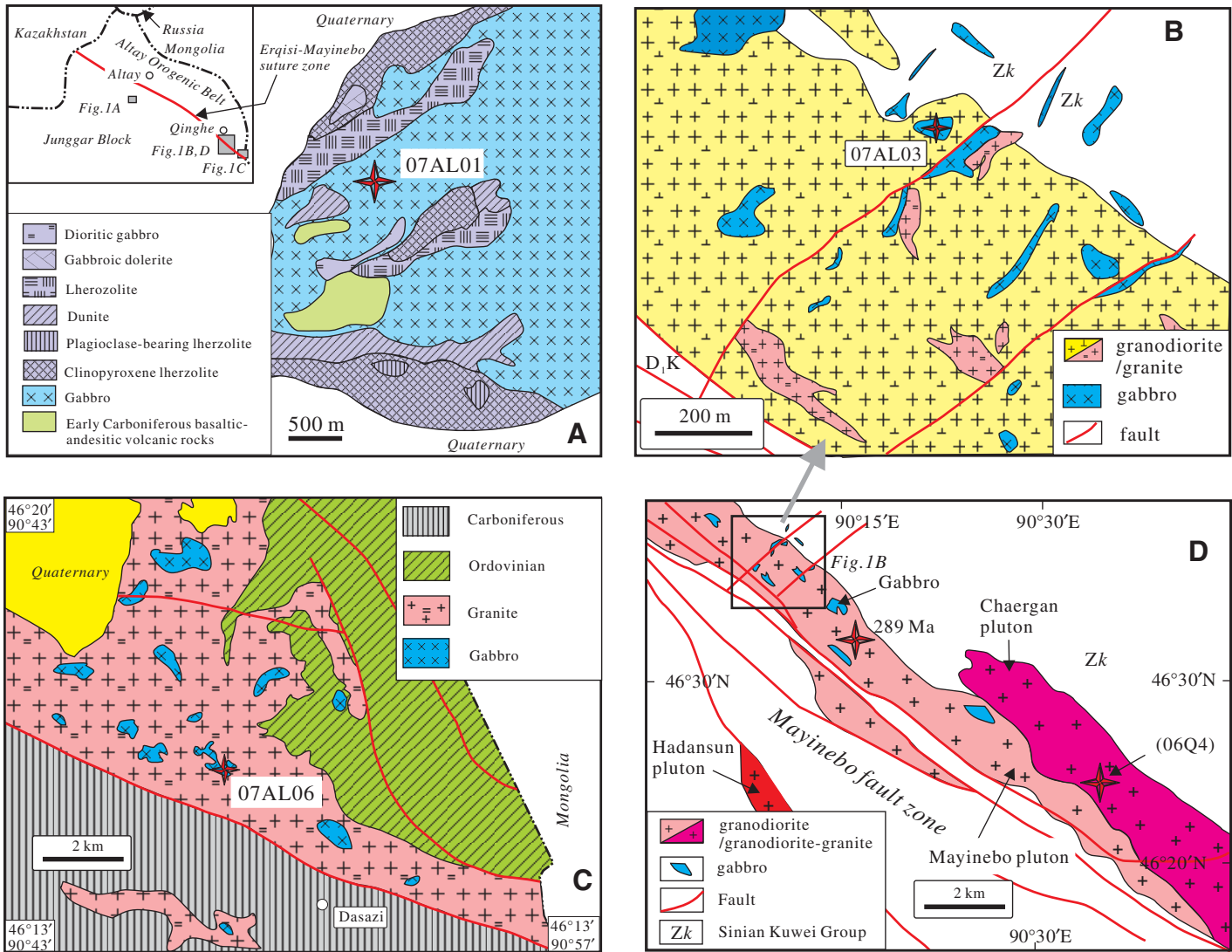


Figure 2. Simplified geological map for (A) the Hongguleneng ultramafic-mafic complex (after Bai and Zhou, 1991), (B) the Mayinebo gabbro dikes and plutons, (C) the Dasazi bimodal intrusive complex, and (D) the Chaergan granitic pluton. The northeastern-striking faults in B and C are part of the Mayinebo faults zone. Inset in the upper left corner of A shows the locations of the studied rock bodies.

of plagioclase (25%–50%), microcline (25%–50%), quartz (15%–30%), hornblende (1%–10%), and biotite (1%–5%). Accessory minerals include zircon, apatite, and allanite. The gabbros that mingle with the granites share similar petrography with the Mayinebo gabbro.

Analytical Methods

One geochronological sample each was collected from the Hongguleneng ultramafic-mafic complex (07AL01, 46°47'17"N, 86°24'31"E), the Mayinebo gabbroic intrusion (07AL03, 46°35'8"N, 90°11'57"E), the Dasazi bimodal intrusion (Dasazi gabbro-granite complex) (07AL06, 46°15'34"N, 90°48'45"E), and the Chaergan granitic pluton (06Q4, 46°31'10"N,

88°21'35"E). Mineral separation was carried out first using conventional magnetic and density techniques to concentrate the nonmagnetic, heavy fractions. Zircon grains were then extracted by handpicking under a binocular microscope. Zircon ages were analyzed using the SHRIMP U-Pb method. Zircon grains were cast into an epoxy mount, which was then polished to section the crystals in half for analysis. Zircons were documented with transmitted and reflected light photomicrographs and cathodoluminescence (CL) images to reveal their inner structures. Before measurement, the mount was vacuum-coated with high-purity gold. U-Th-Pb analyses of samples 07AL01, 07AL03, and 07AL06 were conducted using the SHRIMP II (A) ion microprobe at Curtin

University of Technology under standard operating conditions (Williams, 1998), and sample 06Q4 was analyzed in the Beijing SHRIMP Centre, Chinese Academy of Geological Sciences. U-Th-Pb ratios were determined relative to the 91500 standard zircon, and the U and Th absolute abundances were determined relative to the SL13 standard zircon. Measured compositions were corrected for common Pb using nonradiogenic ^{204}Pb , and an average crustal composition (Stacey and Kramers, 1975) appropriate to the age of the mineral was assumed. Software SQUID 1.0 and ISOPLOT (Ludwig, 1999, 2001) were used for data processing. The weighted mean ages are quoted at 95% confidence level. U-Pb zircon data are presented in Table 1.

TABLE 1. SENSITIVE HIGH-RESOLUTION ION MICROPROBE (SHRIMP) U-Pb DATA FOR ZIRCONS FROM THE MAFIC AND BIMODAL INTRUSIVE COMPLEX IN SOUTH OF ALTAI

Spot	U (ppm)	Th (ppm)	Th/U	$f_{206}^{\#}$ (%)	$^{206}\text{Pb}^*/^{238}\text{U}$ ($\pm 1\sigma$)	$^{207}\text{Pb}^*/^{235}\text{U}$ ($\pm 1\sigma$)	$^{207}\text{Pb}^*/^{206}\text{Pb}^*$ ($\pm 1\sigma$)	$^{206}\text{Pb}/^{238}\text{U}$ age (Ma) ($\pm 1\sigma$)	$^{207}\text{Pb}/^{206}\text{Pb}$ age (Ma) ($\pm 1\sigma$)					
07AL01 (Hongguleng mafic-ultramafic complex)														
1.1	160	84	0.54	0.18	0.0445	2.0	0.31	4.3	0.0513	3.8	280.5	5.6	258	86
2.1	103	61	0.61	0.48	0.0800	2.1	0.54	5.3	0.0492	4.9	496.2	10.1	162	113
3.1	717	602	0.87	0.00	0.0438	1.9	0.31	2.4	0.0515	1.5	276.3	5.1	262	34
4.1	114	57	0.52	0.00	0.0424	2.1	0.31	4.3	0.0526	3.7	267.6	5.5	313	85
5.1	162	104	0.66	0.16	0.0428	2.1	0.27	5.9	0.0451	5.5	270.3	5.6	-50	133
6.1	607	591	1.01	-0.07	0.0425	1.9	0.31	2.5	0.0535	1.7	268.3	5.0	350	38
7.1	927	927	1.03	0.16	0.0425	1.9	0.30	2.7	0.0509	1.9	268.3	5.0	238	44
8.1	234	158	0.70	-0.13	0.0436	2.0	0.31	3.4	0.0520	2.7	275.2	5.4	285	62
9.1	303	225	0.76	0.46	0.0440	2.0	0.31	4.5	0.0520	4.1	277.3	5.4	288	91
10.1	651	165	0.26	0.21	0.0438	1.9	0.31	2.7	0.0511	2.0	276.2	5.2	248	45
11.1	260	126	0.50	0.00	0.0430	2.2	0.32	4.4	0.0533	3.8	271.4	5.9	343	86
12.1	241	118	0.50	0.13	0.0432	2.0	0.31	3.6	0.0527	3.0	272.9	5.3	315	68
13.1	912	118	0.13	0.16	0.0438	1.9	0.31	2.4	0.0516	1.5	276.6	5.1	267	35
14.1	807	789	1.01	0.04	0.0430	1.9	0.31	2.7	0.0518	1.9	271.6	5.0	279	44
15.1	1261	137	0.11	0.21	0.0422	1.9	0.29	2.5	0.0505	1.6	266.4	4.9	222	37
16.1	504	275	0.56	0.29	0.0439	1.9	0.30	3.5	0.0498	2.9	277.1	5.2	190	67
17.1	145	75	0.54	-0.94	0.0446	2.1	0.37	6.8	0.0598	6.5	281.1	5.8	590	138
18.1	149	72	0.50	-0.31	0.0431	2.1	0.33	3.7	0.0549	3.1	272.1	5.5	407	70
07AL03 (Qingh mafic intrusion or dikes)														
1.1	495	292	0.61	-0.08	0.0449	1.9	0.34	2.8	0.0556	2.0	283.1	5.3	436	44
2.1	1319	11	0.01	0.06	0.0434	1.9	0.31	2.3	0.0510	1.3	274.0	5.1	241	30
3.1	226	71	0.33	0.22	0.0412	2.1	0.28	4.9	0.0494	4.4	260.5	5.3	168	103
4.1	412	405	1.02	-0.07	0.0498	1.9	0.35	2.8	0.0514	2.0	313.5	5.9	257	45
5.1	189	71	0.39	0.89	0.0428	2.1	0.28	8.1	0.0478	7.8	270.5	5.5	91	186
6.1	167	74	0.46	0.71	0.0429	2.2	0.28	6.2	0.0469	5.8	270.6	5.8	43	139
7.1	521	307	0.61	-0.01	0.0422	1.9	0.30	2.8	0.0523	2.0	266.2	5.1	298	45
8.1	481	392	0.84	0.36	0.0423	1.9	0.29	3.6	0.0502	3.1	266.9	5.0	204	72
9.1	363	278	0.79	0.39	0.0434	2.0	0.29	4.1	0.0483	3.6	274.0	5.2	116	85
10.1	444	377	0.88	0.47	0.0419	1.9	0.29	3.5	0.0501	2.9	264.8	5.0	201	67
11.1	409	305	0.77	0.09	0.0435	2.0	0.30	3.2	0.0505	2.6	274.5	5.3	218	59
12.1	419	253	0.62	0.39	0.0446	1.9	0.30	4.1	0.0487	3.6	281.0	5.3	132	85
13.1	431	248	0.59	-0.21	0.0437	1.9	0.32	2.7	0.0538	1.9	275.9	5.2	363	43
14.1	127	45	0.36	1.06	0.0428	2.1	0.26	7.1	0.0433	6.8	270.1	5.6	-151	168
15.1	427	280	0.68	0.35	0.0430	1.9	0.29	3.6	0.0495	3.1	271.3	5.1	170	72
16.1	1222	942	0.80	0.18	0.0435	1.9	0.31	2.5	0.0514	1.7	274.4	5.1	257	38
17.1	669	492	0.76	-0.16	0.0453	1.9	0.33	2.8	0.0525	2.1	285.4	5.3	309	47
18.1	263	158	0.62	0.24	0.0424	2.0	0.31	3.6	0.0522	3.1	267.5	5.2	295	70
19.1	1024	708	0.71	0.02	0.0444	1.9	0.32	2.4	0.0527	1.5	279.9	5.2	314	33
20.1	288	181	0.65	0.41	0.0425	2.0	0.29	4.3	0.0488	3.8	268.3	5.2	139	90
07AL06 (Gabbro from the Dasazi bimodal intrusive complex)														
1.1	395	251	0.66	0.59	0.0445	1.9	0.29	4.3	0.0466	3.8	280.9	5.3	31	91
2.1	259	209	0.83	0.15	0.0418	2.0	0.30	3.3	0.0517	2.7	264.2	5.1	272	62
3.1	458	326	0.74	0.47	0.0431	1.9	0.29	4.3	0.0487	3.8	271.9	5.2	133	90
4.1	677	106	0.16	0.81	0.0432	1.9	0.30	5.4	0.0507	5.0	272.9	5.2	228	116
5.1	279	150	0.56	-0.06	0.0425	2.0	0.30	3.2	0.0519	2.5	268.3	5.2	279	57
6.1	219	15	0.07	0.39	0.0419	2.0	0.27	5.8	0.0465	5.5	264.7	5.2	26	131
7.1	295	128	0.45	1.09	0.0432	2.0	0.31	6.3	0.0523	5.9	272.4	5.3	298	135
8.1	898	65	0.08	0.08	0.0433	1.9	0.30	2.4	0.0504	1.4	273.0	5.1	214	33
9.1	266	134	0.52	0.91	0.0420	2.0	0.32	6.6	0.0549	6.3	265.0	5.2	409	141
10.1	360	186	0.53	0.77	0.0430	2.0	0.29	4.9	0.0488	4.5	271.4	5.2	138	106
11.1	142	16	0.11	0.91	0.0439	2.1	0.31	2.1	0.0520	9.9	277.0	5.8	286	226
12.1	272	30	0.11	0.38	0.0430	2.0	0.31	4.1	0.0518	3.6	271.4	5.2	275	82
13.1	213	132	0.64	0.54	0.0434	2.0	0.28	5.2	0.0470	4.8	273.7	5.4	48	116
14.1	217	132	0.63	0.78	0.0424	2.0	0.28	5.2	0.0472	4.8	267.5	5.2	61	115
15.1	142	52	0.38	0.52	0.0422	2.1	0.27	6.1	0.0459	5.8	266.3	5.4	-9	139
16.1	463	352	0.79	0.42	0.0420	1.9	0.28	4.0	0.0484	3.5	265.4	5.0	121	83
17.1	210	99	0.48	0.19	0.0407	2.0	0.29	3.7	0.0509	3.1	257.3	5.0	235	72
06Q4 (Chaergan granite)														
1.1	286	80	0.29	1.19	0.04288	2.3	0.250	26	0.042	26	270.7	6.1	-211	642
2.1	344	98	0.30	17.24	0.04392	2.0	0.256	15	0.0422	15	277.1	5.3	-213	374
3.1	486	100	0.21	6.30	0.04462	1.8	0.324	6.1	0.0527	5.8	281.4	5.0	314	133
4.1	686	253	0.38	3.07	0.04299	1.8	0.321	5.3	0.0541	5.0	271.3	4.7	376	113
5.1	353	76	0.22	2.71	0.05277	1.9	0.416	6.0	0.0572	5.7	331.5	6.1	498	125
6.1	390	153	0.41	0.76	0.04348	2.0	0.272	13	0.0453	13	274.4	5.3	-38	305
7.1	317	110	0.36	0.80	0.0485	2.1	0.311	18	0.0464	17	305.6	6.2	20	420
8.1	630	151	0.25	1.15	0.04357	1.8	0.326	7.9	0.0542	7.6	274.9	4.9	379	172
9.1	253	198	0.81	2.14	0.0440	2.3	0.309	22	0.051	22	277.3	6.3	241	507
10.1	401	100	0.26	3.07	0.04480	1.9	0.323	7.2	0.0523	6.9	282.5	5.1	301	158
11.1	686	240	0.36	1.34	0.04417	1.8	0.304	6.7	0.0499	6.5	278.6	4.8	191	150
12.1	242	102	0.43	2.68	0.0454	2.3	0.303	21	0.048	21	286.4	6.4	118	492
13.1	657	141	0.22	1.07	0.04381	1.8	0.306	5.5	0.0507	5.2	276.4	4.9	228	120

*Pb is radiogenic lead.

[#]f₂₀₆ is percentage of common ²⁰⁶Pb in total ²⁰⁶Pb.

TABLE 2. MAJOR- AND TRACE-ELEMENT COMPOSITIONS OF THE ULTRAMAFIC INTRUSION, BIMODAL INTRUSIVE COMPLEX, AND MAFIC INTRUSIONS IN SOUTH BELT OF ALTAI

Sample: Rock type:	Hongguleneng complex						Mayinebo gabbro			
	AL01 GB	AL05 GB	AL06 OGB	AL07 OGB	AL08 GB	AL010 OGB	07AL3-1 GB	07AL03-2 GB	07AL03-3 GB	07AL03-4 GB
Major elements (%)										
SiO ₂	41.25	41.69	39.54	43.02	43.62	39.96	49.08	46.27	48.70	46.65
Al ₂ O ₃	20.30	17.86	12.16	9.48	15.84	11.44	18.36	16.95	17.56	16.56
CaO	13.57	10.27	7.17	8.83	13.98	15.57	9.40	9.19	9.48	8.80
Fe ₂ O ₃	3.74	5.77	7.58	9.30	5.93	5.84	8.77	9.27	9.90	10.03
K ₂ O	0.01	0.01	0.01	0.02	0.04	0.00	0.15	0.13	0.19	0.13
MgO	13.18	17.83	25.01	23.96	14.99	19.76	10.05	14.09	9.65	13.85
MnO	0.06	0.08	0.11	0.14	0.10	0.13	0.14	0.14	0.15	0.15
Na ₂ O	0.61	0.85	0.44	0.69	0.86	0.13	2.79	2.64	2.90	2.57
P ₂ O ₅	0.01	0.01	0.01	0.01	0.01	0.01	0.09	0.06	0.09	0.06
TiO ₂	0.05	0.04	0.04	0.14	0.12	0.31	0.88	0.64	1.10	0.71
LOI	7.23	5.46	8.28	4.25	4.70	6.86	0.31	0.05	0.22	0.09
Total	100.02	99.85	100.33	99.83	100.18	100.01	100.03	99.42	99.95	99.59
Trace elements (ppm)										
Sc	5.01	5.39	7.94	25.98	21.70	26.68	19.82	16.67	23.19	13.83
V	40.7	48.2	51.4	116.2	95.8	231.6	182.2	142.7	210.4	164.2
Cr	719	1458	2822	1203	593	1214	353	755	302	706
Co	40.82	59.23	75.99	80.57	55.13	39.67	46.95	59.18	47.54	60.87
Ni	485	624	1027	743	457	427	234	409	208	398
Cu	40.0	65.9	128.9	107.6	90.5	82.1	34.9	45.1	40.3	48.5
Zn	65.0	41.0	63.2	47.7	36.4	37.7	56.3	56.8	67.8	91.0
Ga	9.19	8.92	6.21	6.52	9.69	4.27	16.9	15.2	17.3	15.3
Rb	2.21	0.73	0.85	1.44	0.92	0.35	5.61	4.27	5.88	4.17
Sr	581	448	109	179	508	15	327	273	326	259
Y	1.79	0.90	0.89	3.58	3.13	8.34	12.63	10.18	14.26	10.46
Zr	8.72	1.84	1.13	4.35	3.63	8.98	56.81	36.55	65.62	42.45
Nb	0.33	0.31	0.10	0.13	0.14	0.13	2.65	1.55	3.04	1.52
Mo	2.82	2.37	1.22	1.07	3.12	1.91	1.40	2.17	1.63	2.96
Cd	0.07	0.06	0.07	0.08	0.09	0.14	0.16	0.12	0.15	0.14
Sn	1.43	0.20	0.19	0.28	0.52	0.73	1.05	1.05	1.17	1.11
Cs	0.18	0.16	0.12	0.07	0.11	0.02	0.99	0.41	0.83	0.60
Ba	1613	396	41.8	17.3	88.2	5.8	31.8	23.4	35.8	23.1
La	0.80	0.17	0.19	0.31	0.27	0.56	5.24	3.36	5.61	3.38
Ce	1.58	0.39	0.38	0.73	0.71	1.49	10.70	7.09	11.48	7.17
Pr	0.22	0.05	0.05	0.13	0.12	0.26	1.42	0.98	1.53	0.98
Nd	0.93	0.28	0.25	0.74	0.66	1.58	6.95	4.91	7.27	5.13
Sm	0.22	0.10	0.07	0.30	0.27	0.70	1.93	1.44	1.96	1.52
Eu	0.21	0.12	0.07	0.17	0.21	0.41	0.86	0.66	0.90	0.66
Gd	0.42	0.18	0.12	0.48	0.43	1.12	2.31	1.81	2.48	1.80
Tb	0.05	0.02	0.02	0.08	0.07	0.20	0.34	0.28	0.38	0.28
Dy	0.37	0.17	0.16	0.69	0.60	1.57	2.51	1.99	2.78	2.05
Ho	0.08	0.04	0.04	0.16	0.13	0.38	0.55	0.44	0.61	0.46
Er	0.20	0.11	0.11	0.46	0.39	1.05	1.50	1.24	1.71	1.28
Tm	0.03	0.02	0.02	0.07	0.06	0.16	0.22	0.17	0.26	0.19
Yb	0.17	0.11	0.11	0.40	0.35	0.90	1.34	1.06	1.52	1.10
Lu	0.03	0.02	0.02	0.06	0.05	0.14	0.21	0.16	0.24	0.17
Hf	0.26	0.05	0.05	0.18	0.14	0.41	1.56	1.06	1.74	1.17
Ta	0.08	0.08	0.03	0.05	0.05	0.05	0.28	0.26	0.24	0.17
Bi	0.02	0.01	0.01	0.01	0.02	0.02	0.01	0.02	0.01	0.02
Th	0.16	0.06	0.09	0.07	0.05	0.05	0.92	0.58	0.85	0.53
U	0.05	0.02	0.02	0.02	0.01	0.02	0.28	0.21	0.25	0.18

(continued)

Contents of major-element oxides were obtained using a Rigaku ZSX100e X-ray fluorescence (XRF) spectrometer and fused glass beads at the Guangzhou Institute of Geochemistry of the Chinese Academy of Sciences, following analytical procedures similar to those of X.H. Li et al. (2006). Analytical precision was between 1% and 5%. Trace elements were analyzed using a Finnigan ELEMENT inductively coupled plasma-mass spectrometer (ICP-MS) at Nanjing University, following a procedure similar to those described by X.H. Li et al. (2000). About 50 mg sample powders from each sample were dissolved in high-pressure Teflon bombs using HF + HNO₃ mixture. An internal standard solution containing single-element Rh was used

for monitoring signal drift during ion counting. U.S. Geological Survey standards BCR-1, W-2, and G-2 and Chinese National standards GSR-1 and GSR-3 were used for calibrating element concentrations of the unknowns. In-run analytical precisions for most elements were generally better than 2%–5%. The analytical results of major and trace elements are listed in Table 2. Sr-Nd isotopes were determined using a Micromass Isoprobe multicollector ICP-MS (MC-ICP-MS) at Nanjing University following the procedure described by X.H. Li et al. (2006). Measured ⁸⁷Sr/⁸⁶Sr and ¹⁴³Nd/¹⁴⁴Nd ratios were normalized to ⁸⁶Sr/⁸⁸Sr = 0.1194 and ¹⁴⁶Nd/¹⁴⁴Nd = 0.7219, respectively. The reported ⁸⁷Sr/⁸⁶Sr and ¹⁴³Nd/¹⁴⁴Nd ratios were adjusted to

the NBS SRM 987 standard ⁸⁷Sr/⁸⁶Sr = 0.71025 and the Shin Etsu JNdi-1 standard ¹⁴³Nd/¹⁴⁴Nd = 0.512115, respectively. Sr-Nd isotope results are listed in Table 3.

Analytical Results

Geochronology

Hongguleneng Gabbro. Zircon grains from gabbro sample 07AL01 are typically euhedral with no visible inherited cores. Eighteen zircon grains were analyzed. Among them, 17 spots have U values ranging from 114 ppm to 1261 ppm, Th ranging from 57 ppm to 798 ppm, and Th/U ratios between 0.11 and 1.03. Their apparent ²⁰⁶Pb/²³⁸U ages range from 267 Ma to

TABLE 2. MAJOR- AND TRACE-ELEMENT COMPOSITIONS OF THE ULTRAMAFIC INTRUSION, BIMODAL INTRUSIVE COMPLEX, AND MAFIC INTRUSIONS IN SOUTH BELT OF ALTAY (continued)

Sample: Rock type:	Mayinebo gabbro						Dasazi complex			
	07AL03-5 GB	07AL03-6 GB	07AL03-7 GB	07AL03-8 GB	07AL03-9 GB	07AL03-10 GB	07AL03-11 GB(coarse)	07AL04-1 GND	07AL04-2 GND	07AL04-3 GND
Major elements (%)										
SiO ₂	48.02	49.14	48.42	46.80	49.30	47.66	54.40	67.19	63.89	62.72
Al ₂ O ₃	17.94	17.96	17.50	16.45	18.25	17.47	14.83	14.96	15.63	14.93
CaO	8.95	9.60	9.53	8.59	9.83	9.34	7.61	2.50	3.18	3.10
Fe ₂ O ₃	8.94	8.96	9.78	10.08	8.71	8.99	7.71	5.42	6.36	7.57
K ₂ O	0.16	0.14	0.19	0.13	0.14	0.22	0.43	2.86	3.33	2.86
MgO	12.11	10.00	9.46	14.02	9.67	10.60	3.46	1.58	1.88	2.17
MnO	0.13	0.14	0.15	0.14	0.14	0.13	0.16	0.09	0.11	0.12
Na ₂ O	2.81	2.90	2.93	2.53	2.98	2.38	6.40	3.22	3.96	3.63
P ₂ O ₅	0.07	0.08	0.14	0.06	0.08	0.07	0.95	0.29	0.32	0.38
TiO ₂	0.76	0.83	1.12	0.69	0.87	0.78	2.13	0.91	1.08	1.26
LOI	0.21	0.03	0.48	0.11	0.12	2.58	2.29	0.46	0.41	0.60
Total	100.10	99.77	99.69	99.59	100.10	100.22	100.35	99.47	100.14	99.36
Trace elements (ppm)										
Sc	15.4	21.7	24.0	16.8	22.7	20.1	25.5	14.5	14.9	17.9
V	150	181	223	158	185	155	238	106	111	134
Cr	751	427	321	680	443	366	21.0	37.1	40.0	49.7
Co	53.8	46.0	46.4	52.7	45.2	44.7	37.4	12.0	11.9	14.4
Ni	342	236	205	404	204	248	51.4	12.4	12.7	17.3
Cu	41.3	34.9	41.0	48.1	36.8	27.0	227	17.9	15.8	17.9
Zn	77.4	57.6	65.6	69.4	51.0	56.8	52.8	71.1	78.5	94.2
Ga	16.0	17.0	18.1	15.2	17.5	15.7	26.6	22.7	24.3	25.1
Rb	5.15	3.27	5.17	3.87	2.47	7.06	12.9	124	130	144
Sr	303	324	328	255	344	271	275	196	211	194
Y	10.4	12.3	16.9	10.4	12.2	10.6	95.5	35.8	42.1	41.0
Zr	44.3	50.0	75.0	37.8	53.2	37.9	574	493	578	674
Nb	2.04	2.08	3.02	1.52	2.22	1.90	17.8	12.6	12.2	15.2
Mo	1.90	1.47	1.48	1.86	1.86	1.21	2.07	1.47	1.78	1.56
Cd	0.12	0.13	0.14	0.12	0.12	0.11	0.45	0.48	0.48	0.50
Sn	0.93	0.92	1.27	1.12	1.04	0.78	2.57	2.83	2.69	2.82
Cs	0.67	0.13	0.96	0.57	0.59	1.47	0.70	4.27	4.04	4.92
Ba	28.9	29.0	35.9	23.0	28.6	31.9	93.7	446	462	327
La	4.20	4.47	6.32	3.26	4.36	3.78	38.8	20.0	26.9	22.4
Ce	8.62	9.10	12.84	6.90	8.84	7.53	81.4	38.9	58.7	43.6
Pr	1.16	1.24	1.75	0.97	1.20	1.05	11.11	5.23	7.40	6.33
Nd	5.62	6.07	8.41	4.81	6.13	5.03	53.4	23.0	30.7	27.9
Sm	1.60	1.80	2.44	1.45	1.72	1.50	14.70	6.15	6.85	7.46
Eu	0.71	0.81	1.00	0.65	0.85	0.73	4.73	1.98	2.05	1.99
Gd	1.90	2.19	3.08	1.81	2.11	1.84	17.80	6.95	7.13	8.55
Tb	0.29	0.33	0.45	0.28	0.32	0.28	2.64	1.14	1.15	1.38
Dy	2.09	2.45	3.33	2.03	2.36	2.13	19.1	8.35	8.73	9.53
Ho	0.45	0.53	0.72	0.45	0.53	0.46	4.09	1.75	1.93	1.96
Er	1.26	1.51	2.00	1.23	1.48	1.29	11.4	4.15	4.87	4.54
Tm	0.18	0.22	0.29	0.19	0.22	0.19	1.68	0.49	0.58	0.51
Yb	1.10	1.27	1.71	1.07	1.29	1.15	10.1	2.65	3.19	2.76
Lu	0.17	0.20	0.27	0.17	0.20	0.18	1.55	0.43	0.50	0.45
Hf	1.27	1.36	1.94	1.06	1.39	1.11	13.4	11.23	13.3	15.4
Ta	0.19	0.16	0.22	0.19	0.22	0.15	0.82	0.70	0.79	0.73
Bi	0.01	0.02	0.02	0.02	0.01	0.05	0.31	0.11	0.09	0.10
Th	0.65	0.58	0.78	0.51	0.49	0.55	5.68	4.30	6.03	4.60
U	0.22	0.18	0.23	0.17	0.14	0.17	2.01	1.51	1.59	1.70

(continued)

281 Ma and form a coherent population within analytical errors (Table 1), yielding a weighted mean ²⁰⁶Pb/²³⁸U age of 273.3 ± 2.6 Ma (mean square of weighted deviates [MSWD] = 0.71; Fig. 3A). This age is significantly younger than the previously reported ca. 626 Ma Sm-Nd isochron age. One zircon (spot 2.1) has an apparent ²⁰⁶Pb/²³⁸U age of 496 Ma, likely representing a xenocryst.

Mayinebo Gabbro. Zircon grains from sample 07AL03 are euhedral, are 100–150 μm in length, and have length/width ratios ranging from 1/1 to 1/3. Among the 20 analyses, 19 analyses form a coherent ²⁰⁶Pb/²³⁸U age population within analytical errors, giving a weighted mean age of 272.5 ± 2.4 Ma (n = 19, MSWD =

1.53; Fig. 3B). This age is regarded as the best estimation for the crystallization age of the gabbro. One zircon (spot 4.1) has an older ²⁰⁶Pb/²³⁸U age (313 Ma), likely representing a xenocryst.

Dasazi Bimodal Intrusive Complex. Zircon grains from gabbro sample 07AL06 are mostly euhedral, transparent, and colorless, are 100–200 μm long, and have length-to-width ratios of 1–3. No inherited zircon core was observed under CL images. Seventeen analyses were conducted on 17 zircon grains (Table 1). One analysis (spot 17.1) showed slight radiogenic Pb loss and was rejected in the age calculation. The remaining 16 analyses are concordant within errors (Fig. 3C), yielding a weighted mean ²⁰⁶Pb/²³⁸U age of 269.4 ± 2.5 Ma (MSWD =

1.14). This age overlaps the unpublished whole-rock Rb-Sr isochron age of 275 ± 12 Ma from the granodiorites (No. 2 Geological Party of Xinjiang B.G.M.R., 1998) and is interpreted as the crystallization age of the Dasazi bimodal complex.

Chaergan Granite. Zircon grains from sample 06Q4 are 150–250 μm long and have length-to-width ratios of 2–4. All the grains are euhedral, transparent, and colorless, with concentric zoning typical of magmatic origin under CL images. No core-rim structure was observed. Thirteen analyses were conducted on 13 zircon grains (Table 1). Among them, two analyses (spots 5.1 and 7.1) have older ²⁰⁶Pb/²³⁸U ages (332 Ma and 306 Ma), and they are likely

TABLE 2. MAJOR- AND TRACE-ELEMENT COMPOSITIONS OF THE ULTRAMAFIC INTRUSION, BIMODAL INTRUSIVE COMPLEX, AND MAFIC INTRUSIONS IN SOUTH BELT OF ALTAY (continued)

Sample: Rock type:	Dasazi complex									
	07AL04-4 GND	07AL04-5 GND	07AL04-6 GND	07AL06-3 GB	07AL06-4 GB	07AL06-5 GB	07AL06-6 GB	07AL06-7 GB	07AL06-8 GB	07AL04-7 GND
Major elements (%)										
SiO ₂	64.49	65.09	65.48	46.15	49.78	46.04	48.07	51.11	47.73	64.63
Al ₂ O ₃	14.97	15.32	15.09	13.36	14.36	13.04	14.61	14.09	13.08	15.33
CaO	3.12	2.83	2.68	8.80	7.23	8.54	7.83	7.03	8.15	2.86
Fe ₂ O ₃	6.72	6.63	5.98	15.36	12.73	16.53	13.74	12.86	14.59	6.51
K ₂ O	2.93	2.94	3.45	0.88	2.14	1.09	1.03	1.95	1.52	2.94
MgO	1.94	1.98	1.77	6.22	4.70	5.57	5.73	3.92	4.95	2.00
MnO	0.11	0.11	0.10	0.18	0.19	0.20	0.19	0.20	0.21	0.11
Na ₂ O	3.74	3.31	3.36	2.85	3.24	2.92	3.29	3.65	3.31	3.43
P ₂ O ₅	0.35	0.37	0.33	0.58	0.91	0.66	0.60	1.66	2.08	0.36
TiO ₂	1.12	1.15	1.01	4.70	3.21	4.73	3.80	2.76	3.69	1.15
LOI	0.54	0.50	0.54	0.39	1.14	0.48	0.80	0.75	0.65	0.53
Total	100.05	100.23	99.80	99.47	99.61	99.78	99.69	99.97	99.96	99.86
Trace elements (ppm)										
Sc	15.7	16.9	14.9	42.2	28.8	42.2	34.3	25.0	29.51	17.5
V	120	130	114	639	383	703	495	344	485	137
Cr	45.6	41.2	39.3	80.8	61.3	14.9	103.6	12.3	17.8	53.3
Co	12.7	13.5	11.7	49.7	32.9	47.9	45.8	26.4	36.1	14.1
Ni	15.13	12.44	11.63	53.46	34.65	23.74	58.65	3.17	4.40	21.2
Cu	16.6	17.5	16.8	60.0	34.4	46.1	41.7	16.7	24.1	19.3
Zn	75.5	82.1	86.7	93.0	134	107	97.3	114	133	88.6
Ga	23.7	24.8	23.3	22.1	25.2	24.3	23.5	26.6	25.4	24.1
Rb	129	140	136	21.2	63.0	23.4	24.7	57.5	37.5	140
Sr	196	191	198	301	322	303	352	330	307	199
Y	37.3	55.9	36.0	41.7	58.0	46.3	40.3	76.8	68.7	44.0
Zr	631	626	522	353	577	394	360	564	507	652
Nb	13.6	14.6	12.3	15.2	22.2	17.6	14.5	24.7	21.0	15.2
Mo	1.91	1.59	2.09	1.74	3.71	2.78	2.42	3.46	3.01	4.10
Cd	0.50	0.49	0.53	0.32	0.49	0.38	0.34	0.49	0.43	0.56
Sn	2.74	3.52	2.73	2.79	4.11	3.33	2.66	4.46	3.65	3.18
Cs	4.43	4.79	4.19	1.40	2.17	1.11	2.35	3.49	1.89	4.82
Ba	332	405	527	145	244	163	161	248	205	366
La	18.4	23.4	25.0	23.5	42.4	28.2	26.0	52.5	46.3	27.9
Ce	35.3	42.5	53.5	58.0	97.8	66.7	60.9	126.1	111.9	61.4
Pr	4.89	6.25	6.60	7.83	12.91	9.03	8.21	16.76	15.54	7.90
Nd	21.9	27.8	27.9	34.6	55.5	39.5	35.8	72.7	70.0	33.4
Sm	6.01	7.59	6.68	8.13	11.8	9.29	8.09	15.66	15.7	8.35
Eu	1.98	2.17	2.04	2.42	3.40	2.77	2.56	4.19	4.22	2.09
Gd	7.17	8.37	7.28	8.85	12.4	9.85	8.72	16.3	16.6	9.19
Tb	1.20	1.47	1.17	1.29	1.76	1.42	1.26	2.26	2.23	1.46
Dy	8.60	11.61	8.31	8.96	12.44	9.89	8.77	15.6	15.4	10.2
Ho	1.71	2.60	1.71	1.89	2.67	2.17	1.92	3.35	3.25	2.10
Er	4.03	6.63	3.97	5.35	7.42	5.99	5.34	9.14	8.80	5.15
Tm	0.49	0.87	0.46	0.77	1.09	0.85	0.78	1.30	1.21	0.60
Yb	2.68	4.72	2.65	4.45	6.45	5.02	4.56	7.64	7.05	2.77
Lu	0.44	0.70	0.42	0.70	1.01	0.79	0.73	1.15	1.09	0.43
Hf	14.1	14.3	11.8	7.66	12.0	8.77	7.70	11.9	10.8	15.4
Ta	0.68	0.90	0.65	1.00	1.38	1.17	1.01	1.67	1.35	0.81
Bi	0.10	0.12	0.10	0.04	0.09	0.06	0.05	0.11	0.07	0.11
Th	3.90	5.32	5.24	2.60	5.21	3.03	2.81	6.48	4.75	6.48
U	1.85	1.96	1.57	0.85	1.78	0.95	0.95	1.81	1.60	1.66

(continued)

xenocrysts. The remaining 11 analyses are concordant within errors (Fig. 3D), yielding a weighted mean ²⁰⁶Pb/²³⁸U age of 277.2 ± 3.2 Ma (MSWD = 0.73). This age is interpreted as the crystallization age of the Chaergan granite.

Elemental Geochemistry

Hongguleng Ultramafic-Mafic Complex.

Six samples were collected from the relatively silicic members of the Hongguleng complex. All samples have high loss-on-ignition values (LOI = 4.3%–8.3%), indicating significant hydrothermal alteration. The elemental data (Table 2) exhibit large compositional ranges, i.e., SiO₂ = 40%–44%, TiO₂ = 0.04%–0.31%, Al₂O₃ = 9.5%–20.3%, CaO = 7.2%–15.6%,

MgO = 15%–25%, Fe₂O₃^T = 3.7%–9.3%, and Cr = 590–2820 ppm. On a Harker diagram, no significant correlation between SiO₂ and other oxides is observed (Fig. 4). Gabbroic members from this complex show a tholeiitic trend on the AFM diagram (Fig. 5), similar to that of almost all the coeval mafic rocks in the Central Asian orogenic belt. As for the trace elements, they contain very low total rare earth element (REE) contents (total REE = 1.6–10.5 ppm) and have variable La_N/Yb_N (0.4–1.34) and significant positive Eu anomalies (δEu = 1.4–2.9) (Table 3; Fig. 6A). Primitive mantle-normalized incompatible element spider diagrams (both chondrite and primitive mantle values are from Sun and McDonough, 1989) exhibit large variations in

contents of incompatible trace elements, reflecting fractional crystallization and accumulation (Fig. 6B).

Mayinebo Gabbro. The geochemistry of the Mayinebo gabbros indicates that they have relatively consistent major- and trace-element compositions, except for the most evolved sample 07AL03–11 (Table 2). On the Harker diagram, Al₂O₃, TiO₂, and CaO increase, and Fe₂O₃ and MgO decrease as SiO₂ increases (Fig. 4). Their major elements are characterized by a tholeiitic trend (Fig. 5), high MgO (9.5%–14.1%) and Al₂O₃ (16.5%–18.4%), and low TiO₂ (0.6%–1.1%) and total alkali contents (2.6%–3.1%, Na₂O > K₂O; Fig. 7A). The 10 mafic samples have low total REE (25–45 ppm), coherent

TABLE 2. MAJOR- AND TRACE-ELEMENT COMPOSITIONS OF THE ULTRAMAFIC INTRUSION, BIMODAL INTRUSIVE COMPLEX, AND MAFIC INTRUSIONS IN SOUTH BELT OF ALTAY (continued)

Sample: Rock type:	Chaergan pluton									
	D2365 GR	D2374 GR	D2368 GND	D2392 PG	D2367 GR	D2373 GND	D2375 GND	D2376 GND	48yQ-1 GND	48yQ-2 GND
Major elements (%)										
SiO ₂	68.84	71.07	65.71	73.47	67.69	65.33	65.78	64.66	65.53	65.21
Al ₂ O ₃	13.68	13.55	14.79	13.91	13.27	14.54	14.86	14.32	14.56	14.6
CaO	2.45	1.93	2.82	1.4	2.58	3.4	3.11	3.21	2.65	2.66
Fe ₂ O ₃	4.12	3.15	5.62	1.66	5.59	5.4	5.37	6.47	6.34	6.36
K ₂ O	4.43	4.46	3.23	4.54	3.36	3.86	3.28	3.36	3.38	3.54
MgO	1.05	0.9	1.93	0.55	2.01	1.43	1.71	2.05	1.59	1.61
MnO	0.09	0.08	0.11	0.06	0.12	0.12	0.1	0.14	0.116	0.099
Na ₂ O	3.57	3.45	3.73	3.19	3.12	3.93	3.69	3.56	3.88	3.67
P ₂ O ₅	0.25	0.18	0.32	0.11	0.31	0.39	0.32	0.37	0.3	0.34
TiO ₂	0.71	0.47	0.82	0.16	0.71	0.99	0.9	1.07	0.972	0.976
LOI	0.58	0.47	0.54	0.62	0.57	0.57	0.72	0.55	0.52	0.5
Total	99.77	99.71	99.62	99.67	99.33	99.96	99.84	99.76	99.84	99.56
Trace elements (ppm)										
Cr	14.6	16	38.4	—	40.6	23.2	35.7	40.7	19.9	19.6
Rb	154	187	114	171	129	127	134	126	156	119
Sr	140	130	200	85.5	185	214	195	201	188	223
Y	58	28.1	49.1	35	46.1	70.5	28.1	46.5	60.8	43.2
Zr	326	226	351	105	312	451	382	404	373	376
Nb	19.3	10.5	16.4	11.3	17	20.3	12.8	15	20.7	14.9
Ba	343	395	513	325	486	506	446	485	406	523
La	51.2	34.6	29.5	23.9	41.6	66.6	46.2	27.8	29.5	37.6
Ce	95.3	49.1	44.1	71.53	69.9	103	65.2	46.8	61.1	70.8
Pr	12.8	8	6.2	8.16	8.6	13.9	9.8	10.1	9.5	9.88
Nd	51.3	28.9	25.3	26.85	37.7	63.2	44.2	38	41.5	43.3
Sm	10.1	5.1	5.5	6.08	8.8	12.3	8.5	6.6	10.9	9.91
Eu	1.9	0.94	0.29	0.87	1.7	2.8	2.1	1.8	2.11	2.17
Gd	11.1	5.5	6	5.95	8.4	13	8.8	7.4	10.9	8.73
Tb	1.9	0.96	1.2	1.14	1.4	2.4	1.5	1.4	1.96	1.56
Dy	10.3	5.2	9.9	6.7	12.9	14.9	10.5	5.5	14.6	10.6
Ho	2.3	1	1.5	1.29	1.5	2.6	1.7	1.6	2.89	2.06
Er	7.8	3.2	6.3	4.11	5.8	8.7	5.8	4.1	8.84	5.56
Tm	0.96	0.46	1.1	0.62	0.87	1.35	0.93	0.46	1.23	0.8
Yb	7.4	2.9	7.2	4.05	4.9	8	6	3.5	7.68	4.61
Lu	1	0.45	0.85	0.56	0.48	0.91	0.71	0.67	1.11	0.7
Hf	10.8	7.3	11.9	3.4	11.1	13.4	12.7	13.1	8.6	10.2
Ta	2.2	1.5	2.5	1.4	1.7	2.7	1.8	1.8	2.35	1.75
Th	14.4	17.1	8.3	14.6	13.7	15.8	8.8	11.4	20.5	29

Note: LOI—loss on ignition; GB—gabbro; OGB—olivine (-bearing) gabbro; GND—granodiorite; GR—granite; PG—potassic granite.

TABLE 3. Sr-Nd ISOTOPE COMPOSITIONS OF THE STUDIED INTRUSIVE ROCKS

Sample	Sm (ppm)	Nd (ppm)	¹⁴⁷ Sm/ ¹⁴⁴ Nd	¹⁴³ Nd/ ¹⁴⁴ Nd ±	2σ _m	ε _{Nd} (t)	Rb (ppm)	Sr (ppm)	⁸⁷ Rb/ ⁸⁶ Sr	⁸⁷ Sr/ ⁸⁶ Sr	2σ _m	(⁸⁷ Sr/ ⁸⁶ Sr) _i
<i>Mayinebo gabbros</i>												
07AL3-3	1.96	7.27	0.1630	0.512798	2	4.3	5.88	326	0.051	0.704492	4	0.7043
07AL3-7	2.44	8.41	0.1754	0.512814	9	4.2	5.17	328	0.044	0.704421	6	0.7043
07AL3-8	1.45	4.81	0.1823	0.512772	5	3.1	3.87	255	0.043	0.704537	2	0.7044
07AL3-11	14.7	53.4	0.1664	0.512778	8	3.8	12.9	275	0.132	0.704892	3	0.7044
<i>Dasazi bimodal intrusive complex</i>												
07AL4-2	6.85	30.7	0.1349	0.512607	4	1.5	130	211	1.743	0.713981	3	0.7073
07AL4-6	6.68	27.9	0.1446	0.512633	6	1.7	136	198	1.944	0.714669	3	0.7072
07AL4-7	8.35	33.4	0.1513	0.512640	6	1.6	140	199	1.992	0.715034	3	0.7074
07AL6-4	11.76	55.5	0.1282	0.512802	5	5.6	63	322	0.551	0.706060	4	0.7039
07AL6-6	8.09	35.8	0.1367	0.512807	2	5.4	24.7	352	0.197	0.704514	8	0.7038
07AL6-7	15.7	72.7	0.1303	0.512778	3	5.0	57.5	330	0.491	0.705648	3	0.7038
<i>Hongguleng complex</i>												
2K-1	8.15	24.9	0.1980	0.513063	2	8.3	NA	NA	NA	NA	NA	NA
2K-2	0.01	0.04	0.1511	0.512831	5	5.7	NA	NA	NA	NA	NA	NA
2K-4	0.20	0.88	0.1374	0.513041	4	8.2	NA	NA	NA	NA	NA	NA
2K-5	0.25	0.76	0.1989	0.513090	5	8.8	NA	NA	NA	NA	NA	NA
2K-6	0.13	0.44	0.1786	0.512990	4	7.7	NA	NA	NA	NA	NA	NA
2K-8	0.22	0.72	0.1847	0.513010	4	7.5	NA	NA	NA	NA	NA	NA
<i>Chaergan granites</i>												
48yQ-1	10.9	41.5	0.1588	0.512825	2	5.0	NA	NA	NA	NA	NA	NA
D2374	5.10	28.9	0.1067	0.512562	3	1.7	NA	NA	NA	NA	NA	NA

Note: Original data are from Huang et al. (1999); ε_{Nd}(t) was recalculated using the age obtained in this study. NA—not analyzed. 2σ_m is two-sigma mean error.

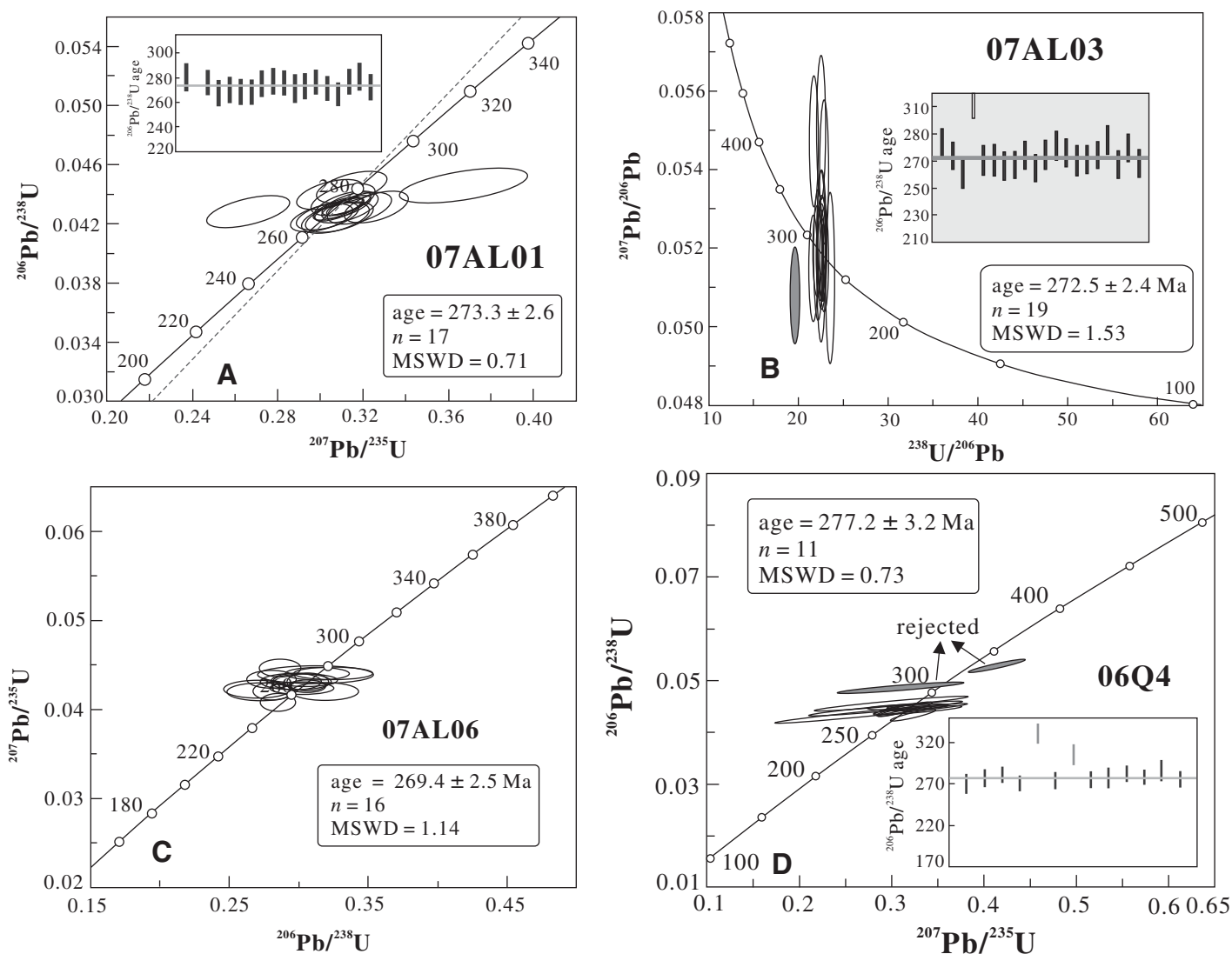


Figure 3. Concordia plots of U-Pb zircon results of the studied intrusive rocks: (A) the Hongguleneng complex, (B) the Mayinebo gabbro, (C) the Dasazi bimodal intrusive complex, and (D) the Chaergan granitic pluton. MSWD—mean square of weighted deviates.

La_N/Yb_N ratios (2.2–2.8), and positive Eu anomalies ($\delta Eu = 1.1$ –1.3) (Fig. 6C). On the primitive mantle-normalized spider diagram, the mafic samples exhibit significant enrichment of Sr and Ba and depletion of Nb-Ta ($Nb/La = 0.4$ –0.5; Fig. 6D). The most evolved sample (07AL03–11) contains relatively high SiO_2 , TiO_2 , P_2O_5 , and most trace elements, but significantly low MgO and Fe_2O_3 contents (Table 2). On the other hand, it shares similar REE and incompatible element distribution patterns, except that it has consistently more elevated values than the other samples, a slightly negative Eu anomaly, and significant negative Sr and Ti anomalies (Fig. 6D).

Dasazi Bimodal Intrusive Complex. The two end members in the Dasazi bimodal intrusive complex show linear trends on the Harker

diagrams (Fig. 4), e.g., as SiO_2 (46%–67%) increases, TiO_2 , CaO, Fe_2O_3 , MgO, and P_2O_5 decrease and Al_2O_3 , Zr, and Rb increase (Fig. 4), indicating mass exchange between them. The gabbroic member exhibits a tholeiitic trend (Fig. 5) and has very high TiO_2 (2.8%–4.7%), Fe_2O_3 (12.7%–16.5%), P_2O_5 (0.6%–2.0%), high total alkali (3.7%–6.4%) (Fig. 7A), total REE (170–340 ppm), and Zr (350–650 ppm) contents but low MgO (3.9%–6.2%), K_2O (0.9%–2.1%), and Rb (21–63 ppm) contents. Chondrite-normalized distribution patterns for gabbros show slight enrichment of light (L) REEs ($La_N/Yb_N = 4$ –5) and moderately negative Eu anomalies ($\delta Eu = 0.8$ –0.9; Fig. 6E). On the primitive mantle-normalized spider diagram, they have significantly negative Sr, Nb, and Ta anomalies relative to neighboring

elements ($Nb/La = 0.45$ –0.65; Fig. 6F). The granodiorites in the complex have consistent major- and trace-element compositions ($SiO_2 = 63.9\%$ –67.2%, $TiO_2 = 0.91\%$ –1.26%, CaO = 2.5%–3.8%, $Al_2O_3 = 14.9\%$ –15.3%, $Fe_2O_3 = 5.4\%$ –7.6%, MgO = 1.6%–2.2%, $Na_2O = 3.2\%$ –4.0%, $K_2O = 2.9\%$ –3.4%, $P_2O_5 = 0.29\%$ –0.37%, Zr = 490–670 ppm, and Rb = 124–144 ppm; Fig. 3). Their major elements indicate peraluminous characteristics ($A/CNK = 0.98$ –1.15; Fig. 7B). On the SiO_2 versus $K_2O + Na_2O$ diagram, they are plotted in the granodiorite area (Fig. 7B). They have total REE ranging from 121 to 172 ppm, are systematically enriched in LREE ($La_N/Yb_N = 5$ –7), and have negative Eu anomalies, with δEu ranging from 0.7 to 0.9 (Fig. 6E). On the primitive mantle-normalized diagram, they show similar patterns

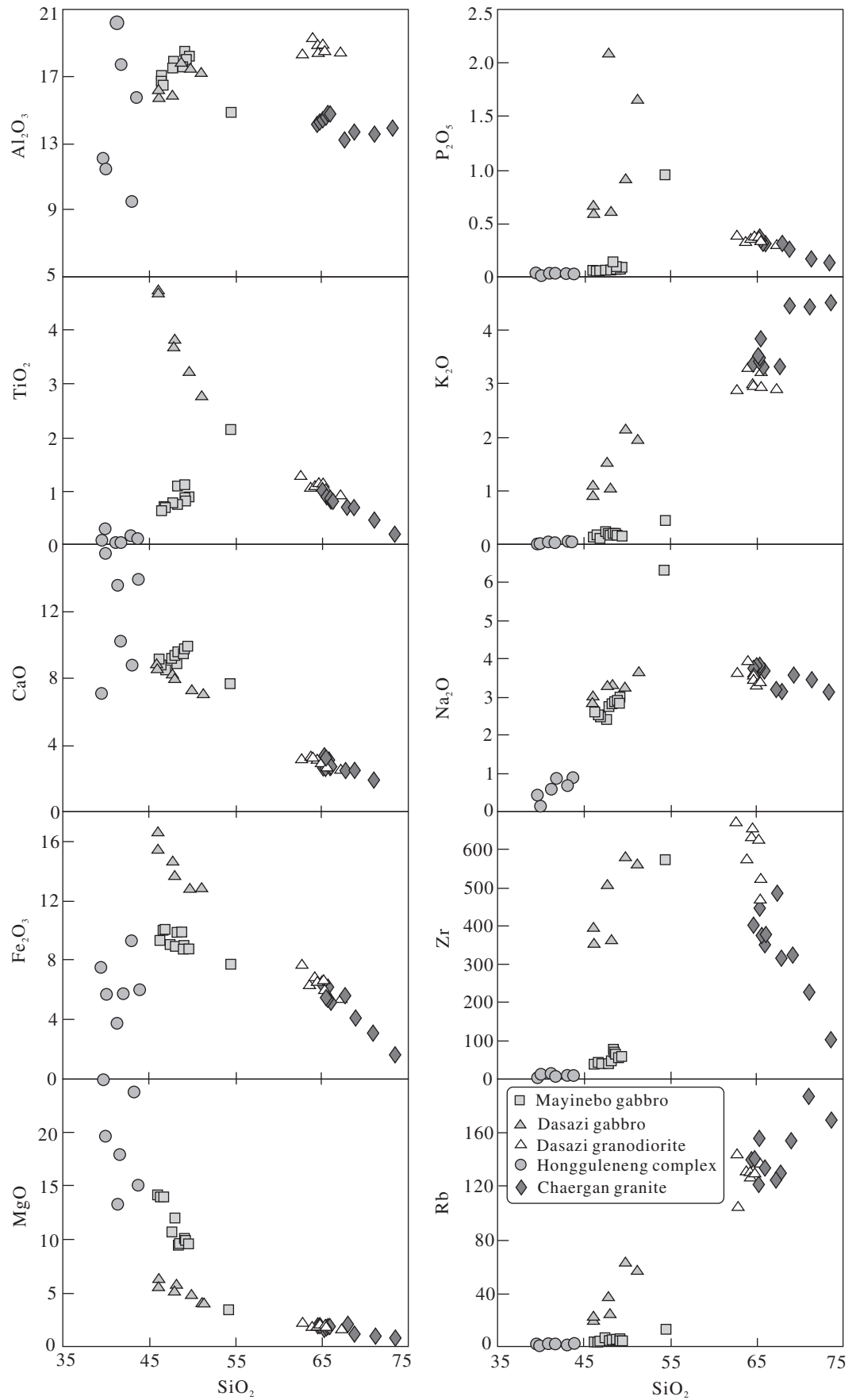


Figure 4. Binary Harker diagrams (SiO_2 versus Al_2O_3 , CaO , MgO , Fe_2O_3 , TiO_2 , Na_2O , K_2O , P_2O_5 , Zr , and Rb) for the studied rocks (see detailed discussion in the text).

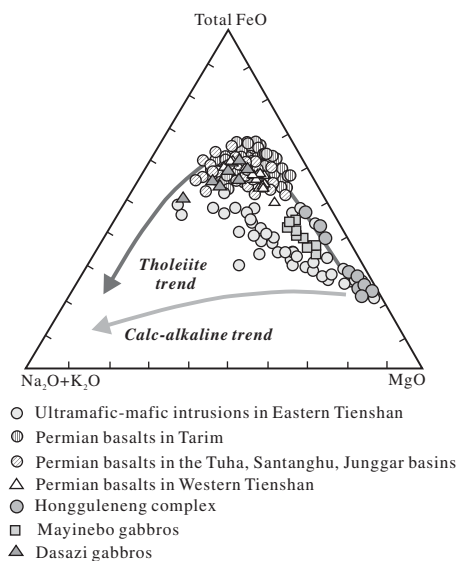


Figure 5. AFM ($\text{Na}_2\text{O} + \text{K}_2\text{O}-\text{FeO}^{\text{T}}-\text{MgO}$) diagram showing the Hongguleneng complex, the Mayinebo gabbros, and the Dasazi gabbros exhibiting tholeiitic trends ($\text{FeO}^{\text{T}} = \text{Fe}_2\text{O}_3^{\text{T}}/1.111$). Permian ultramafic-mafic rocks and basalts in Tarim and Central Asian orogenic belt are also plotted, with original data from D.W. Zhou et al. (2006), Zhou et al. (2004), Jiang et al. (2004a, 2004b), and Zhao et al. (2007).

as the gabbros, except that they have significant depletions in Ti (Fig. 5F).

Chaergan Granitic Pluton. The Chaergan granitic rocks have a large range of major-element compositions: SiO_2 ranges from 64.7% to 73.5%, and TiO_2 , CaO, Fe_2O_3 , MgO, P_2O_5 , and Zr decrease and Rb increases as SiO_2 increases (Fig. 4). Their major elements exhibit metaluminous characteristics ($A/\text{CNK} = 0.86-1.09$), and they plot on the boundary between the alkaline and subalkaline fields (Fig. 7A). They have total REE ranging from 146 ppm to 265 ppm, enrichment of LREE ($L_{\text{a}_N}/Y_{\text{b}_N} = 3-8$), and negative Eu anomalies ($\delta\text{Eu} = 0.5-0.8$) (Fig. 6G). On the primitive mantle-normalized spider diagram, they are enriched in most trace elements but show significant troughs of Nb, P, and Ti (Fig. 6H).

Sr-Nd Isotopic Compositions

Sr-Nd isotopic ratios measured during this study, as well as several results reported by Huang et al. (1999) and recalculated $\epsilon_{\text{Nd}}(t)$ values of the intrusive rocks, are listed in Table 3. The Hongguleneng complex has highly positive $\epsilon_{\text{Nd}}(t)$ values (5.7–8.8) (Huang et al., 1999). The Mayinebo gabbros have positive $\epsilon_{\text{Nd}}(t)$ values ranging from 3.1 to 4.3 and low $(^{87}\text{Sr}/^{86}\text{Sr})_i$ values (0.7043–0.7044). The two end members of

the Dasazi bimodal complex have very different Sr-Nd isotopic compositions, i.e., the gabbros have highly positive $\epsilon_{\text{Nd}}(t)$ (5.0–5.6) and low $(^{87}\text{Sr}/^{86}\text{Sr})_i$ (0.7038–0.7039), whereas the granodiorite has relatively lower, positive $\epsilon_{\text{Nd}}(t)$ (1.5–1.7) and higher $(^{87}\text{Sr}/^{86}\text{Sr})_i$ (0.7072–0.7074). Two samples from the Chaergan pluton have different Nd isotopic compositions: a granodiorite sample has a positive $\epsilon_{\text{Nd}}(t)$ value of 5.0, but a potassic granite sample has a lower positive $\epsilon_{\text{Nd}}(t)$ value of 1.7. In the $\epsilon_{\text{Nd}}(t)$ versus $(^{87}\text{Sr}/^{86}\text{Sr})_i$ diagram, the mafic samples analyzed in this study form evolution trends toward the Permian mafic rocks in the Central Asian orogenic belt (Fig. 8).

Petrogenesis

Hongguleneng Complex

Because all the rocks from the Hongguleneng complex are cumulate products, and no chilled margin or coeval mafic dikes have been found around the complex, it is difficult to decipher its primitive magma composition. However, most rocks have low $L_{\text{a}_N}/Y_{\text{b}_N}$ ratios (less than 1.2) and highly positive $\epsilon_{\text{Nd}}(t)$ values, and so its primitive magma was most likely derived from a time-integrated depleted mantle. On the other hand, most relatively silicic samples have low Nb/La ratios (0.2–0.5), indicating that a depleted mantle source could have been metasomatized by subducted materials shortly before magma generation, and/or the primitive magma could have been contaminated by continental crust. Considering their high positive $\epsilon_{\text{Nd}}(t)$ values and a ca. 496 Ma zircon xenocryst documented by the SHRIMP analyses, metasomatism of the mantle source (major) and crustal contamination (minor) could both have contributed to their low Nb/La ratios. Chemical compositions of the rock-forming minerals suggest that the different members of the Hongguleneng complex are cumulate rocks crystallized from a basaltic magma (e.g., Bai and Zhou, 1991; Peng et al., 1991). Importantly, the Fo numbers of olivine from the complex range from 84 to 91. Using the molar Mg-Fe distribution constant ($K_d = [\text{Fe}/\text{Mg}]^{\text{Oliv}}/[\text{Fe}/\text{Mg}]^{\text{magma}}$) of 0.3 ± 0.03 (Roeder and Emsile, 1970), this suggests a likely high-MgO or picritic primitive magma. On the other hand, chemical compositions of the clinopyroxene from the complex define a typical rifting trend, indicating that the Hongguleneng complex was formed in an intracontinental environment (Fig. 9) (Loucks, 1990).

Mayinebo Gabbros

All the samples are enriched in LREEs and large ion lithophile elements (LILEs) and depleted in heavy (H) REEs and high field strength elements (HFSEs), leading to low Nb/La ratios

(~0.5). On the other hand, they have highly positive $\epsilon_{\text{Nd}}(t)$ values and low $(^{87}\text{Sr}/^{86}\text{Sr})_i$ ratios. Thus, the primary magma of the Mayinebo gabbros was likely derived from a metasomatized lithospheric mantle source. Figure 10 shows that Th/La of the Mayinebo gabbros correlates negatively with Nb/U and Nb/Th, but the correlations of Th/La versus Nb/La and La/Sm are not significant. The average compositions of the continental crust (Rudnick and Gao, 2003), primitive continental arc basalt (Kelemen et al., 2004), and oceanic-island basalt (OIB; Sun and McDonough, 1989) are also shown for reference. The Mayinebo gabbros plot close to primitive continental arc basalts but away from OIB. Further considering their low Ti/Y ratios (Fig. 11), the data suggest that the Mayinebo gabbros were derived from a metasomatized subcontinental mantle source. However, we notice that several samples have relatively higher Nb/La, Nb/U, Nb/Th, and La/Ba (>0.1) ratios than that of the primitive continental arc basalts. Further work is required to determine whether OIB-like magmas were involved in the petrogenesis of the Mayinebo gabbros.

Dasazi Bimodal Intrusive Complex

Gabbros from this bimodal complex have very different chemical compositions from that of the Mayinebo gabbros, e.g., they contain much higher TiO_2 , Fe_2O_3 , Zr, and Rb contents and Ti/Y ratios (300–670) (Figs. 5 and 11). The well-defined linear correlations between TiO_2 , Fe_2O_3 , MgO, and Rb in both the gabbros and granodiorites (Fig. 4), in combination with field observations, strongly argue for mass exchanges between the two end members. Thus, gabbroic samples with low Ti/Y ratios could be due to contamination by the silicic magma (Fig. 11). In Figure 10, the Dasazi gabbros lie between OIB and primitive continental arc basalts. Generally, pure partial melting of a metasomatized subcontinental mantle could not produce high-Ti basalts, e.g., most basalts formed in arc environment are low-Ti series (Pearce and Cann, 1973). Thus, we suggest that the primitive magma of the Dasazi gabbros could have at least partially derived from the asthenospheric mantle. This conclusion is consistent with their positive $\epsilon_{\text{Nd}}(t)$ values and low $(^{87}\text{Sr}/^{86}\text{Sr})_i$ ratios (Table 3; Fig. 8). Contamination of silicic magma can explain the incompatible elemental ratios (e.g., lowered Nb/La and Nb/Th ratios) and Sr-Nd isotopic compositions. This is the first time that high-Ti basaltic rock has been found in the western part of the Central Asian orogenic belt.

The Dasazi granodiorites have high TiO_2 , Fe_2O_3 , MgO, Zr (500–670 ppm), and $\text{Na}_2\text{O}/\text{K}_2\text{O}$ ratios (>1.0) but low Rb/Sr (<0.8). These features, in combination with their petrography,

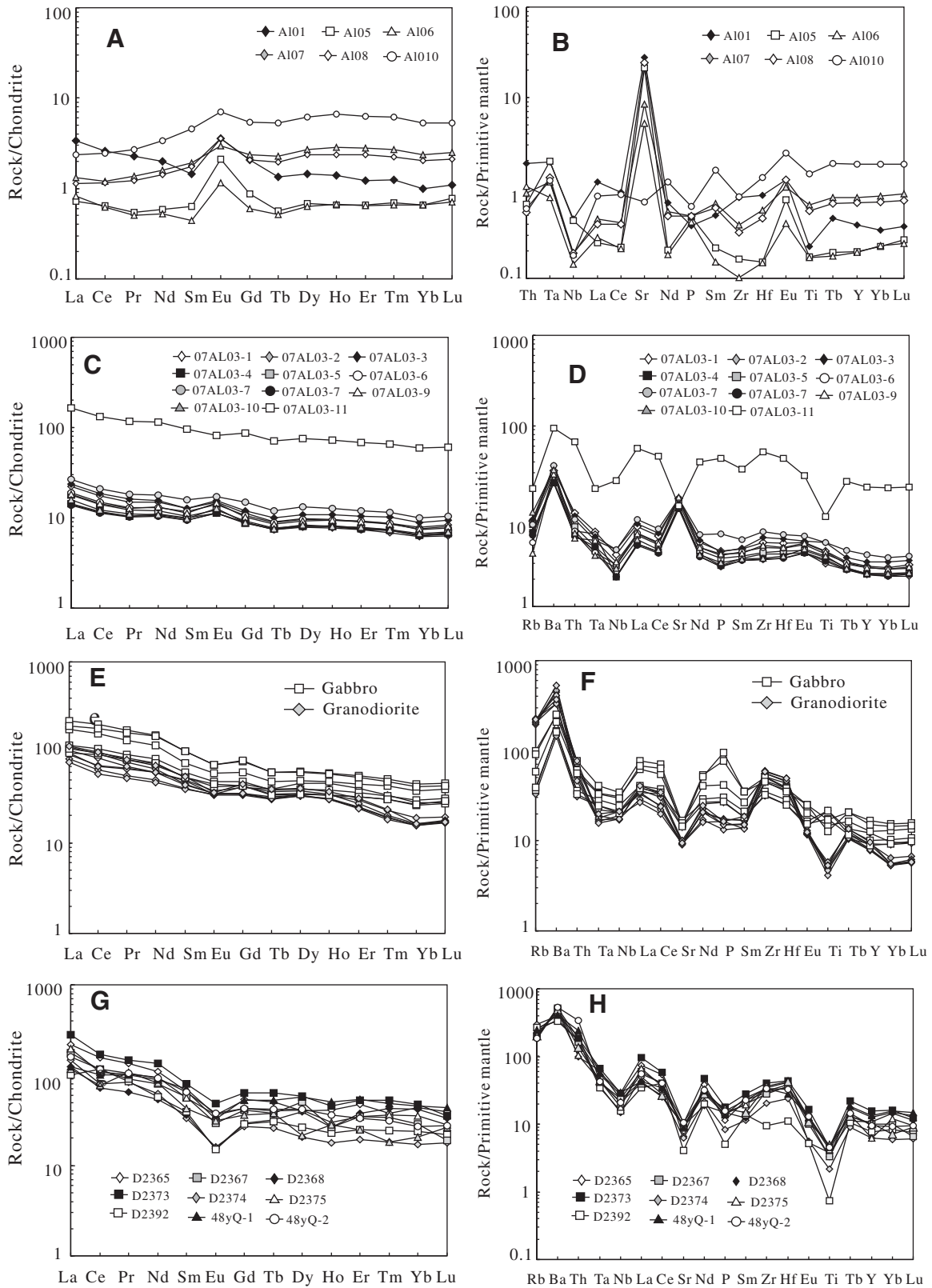
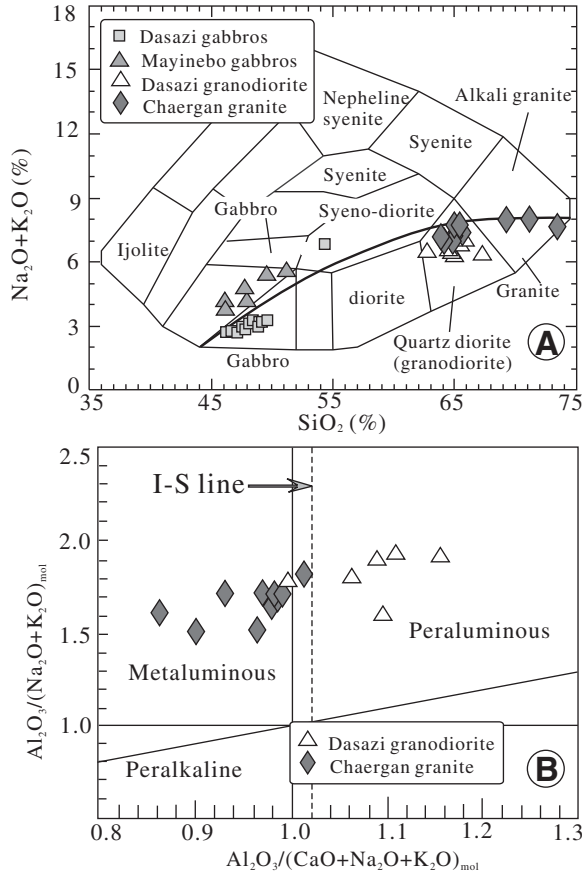


Figure 6. Chondrite-normalized rare earth element (REE) patterns and granodiorite and primitive mantle-normalized incompatible elements spider diagrams for (A, B) Hongguleneng complex, (C, D) Mayinebo gabbros, (E, F) Dasazi complex, and (G, H) Chaergan granodiorite. The normalized values are from Sun and McDonough (1989).

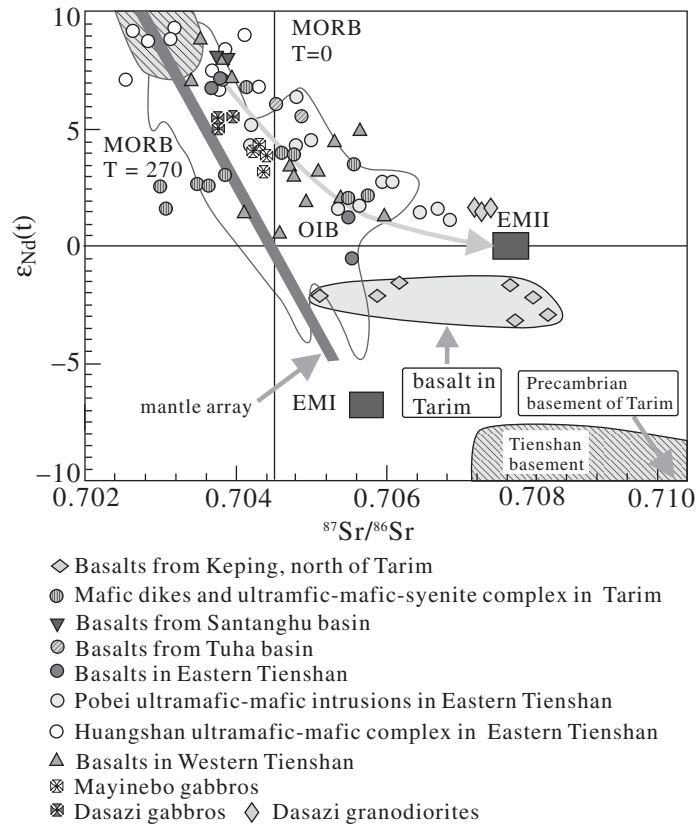
Figure 7. (A) SiO_2 versus $\text{K}_2\text{O} + \text{Na}_2\text{O}$ classification diagram (Cox et al., 1979). (B) A/NK versus A/CNK plot (Maniar and Piccoli, 1989) showing the weakly metaluminous to weakly peraluminous nature of the Chaergan granitic rocks and peraluminous nature of the Dasazi granodiorite. A = Al_2O_3 , N = Na_2O , K = K_2O , C = CaO (all in molar proportion; symbols are same with those in Fig. 4).



suggest that the granodiorites share characteristics of postorogenic to anorogenic granites, i.e., the Peralkaline and alkaline (PAG-type) granites (Barbarin, 1996, 1999). Some geochemical characteristics of the granodiorites also resemble those of A-type granites, such as high Zr and $10,000 \times \text{Ga}/\text{Al}$ ratios (2.8–3.0) and FeO^7/MgO molar ratios (mostly >7) (Whalen et al., 1987). The aforementioned geochemistry precludes the granodiorites from being derived from partial melting of pelitic sources or metagraywackes (Montel and Vielzeuf, 1997). The low K_2O and low Rb/Sr ratios preclude significant mica in their source. A lack of upwardly concave, chondrite-normalized REE patterns indicates that amphibole was not a major residual phase during their formation (Borg and Clyne, 1998), consistent with a hornblende dehydration melting reaction.

Hornblende is abundant in mafic to intermediate igneous and metamorphic rocks, and recent experiments and case studies have revealed that significant proportions (25%–47%) of melt can be generated from basaltic or tonalitic sources by dehydration melting (Petcovic and Grunder, 2003; Sisson et al., 2005). Compared to partial melts derived from mica-rich pelite and graywacke, those formed by dehydration melting of amphibolite generally have lower Al_2O_3 and K_2O and higher CaO (Rapp and Watson, 1995;

Figure 8. $(^{87}\text{Sr}/^{86}\text{Sr})$ versus $\epsilon_{\text{Nd}}(t)$ of the Permian igneous rocks in Tarim, Tianshan, the Santanghu Basin, the Tuha Basin, and Altai (original data are from Jiang et al., 2004a, 2004b, 2006; Zhou et al., 2004; C.L. Zhang et al., 2008; Zhao et al., 2007; Huang et al., 1999; this study; Table 3). MORB—mid-ocean-ridge basalt; OIB—oceanic-island basalt; EMI—I-type enriched mantle; EMII—II-type enriched mantle.



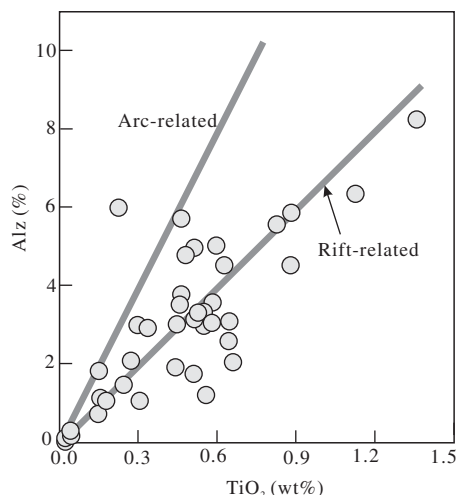


Figure 9. Alz (percentage of tetrahedral sites occupied by Al) versus TiO_2 (wt%) in clinopyroxene from the Hongguleneng ultramafic-mafic complex. Original data of the clinopyroxene are from Bai and Zhou (1989). Reference lines of arc-related and rift-related tectonic environments are from Loucks (1990).

Gerdes et al., 2002). All the analyzed samples from the Dasazi granodiorites have low molar $\text{Al}_2\text{O}_3/(\text{MgO} + \text{FeO}^T)$ ratios (<1.0), indicating that they were derived from partial melting of a mafic precursor, which is consistent with their positive $\epsilon_{\text{Nd}}(t)$ values (1.3–1.5).

Chaergan Granites

The Chaergan granites have a relatively large range of Rb/Sr (0.6–2.0), $\text{Al}_2\text{O}_3/(\text{MgO} + \text{FeO}^T)$ (0.8–3.4), and FeO^T/MgO (5–10) ratios and Zr contents (230–450 ppm). Their $\text{K}_2\text{O}/\text{Na}_2\text{O}$ ratios are a little higher than 1.0. On the ACF diagram, all the samples plot to the I-type granite field (not presented). As for the Nd isotopic compositions, the granodiorite sample and potassic granite sample have very different $\epsilon_{\text{Nd}}(t)$ values. According to their chemical and Nd isotopic characteristics, we suggest that they were derived from partial melting of different sources, including the mafic member and the metagraywacke member. However, on the Rb versus Nb + Y diagram (Pearce et al., 1984), they plot slightly more to the within-plate granite (WPG) field (Fig. 12A).

Tectonic Implications

All the studied intrusive rocks appear to have formed at extensional, or noncompressional settings based on the following evidence: (1) The chemical compositions of clinopyroxene from

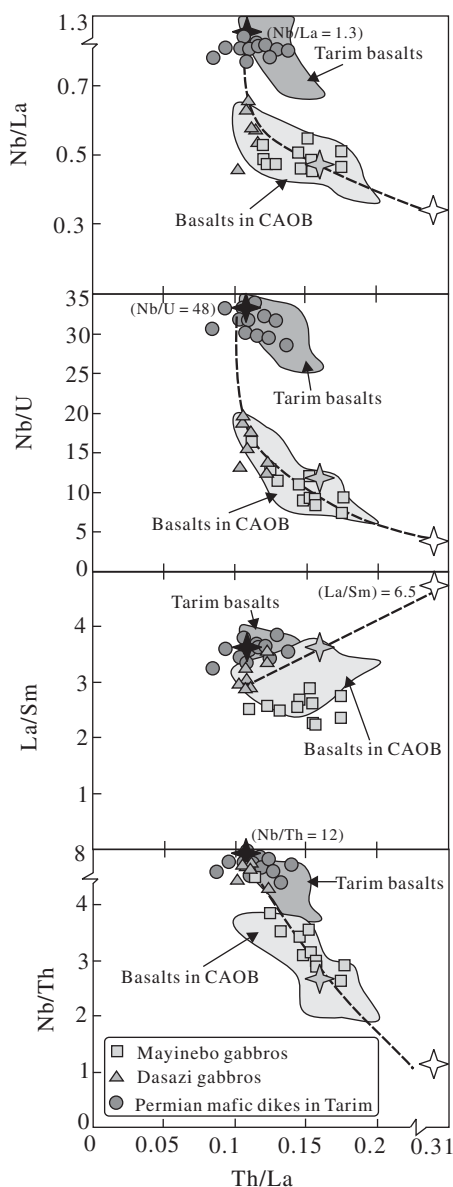


Figure 10. Variations of Nb/U, Nb/Th, Nb/La, and La/Sm with Th/La for the Mayinebo gabbros and the Dasazi gabbros. The open star represents the average composition of the continental crust (Rudnick and Gao, 2003); the yellow star and black star represent the primitive arc basalt and oceanic-island basalt (OIB), respectively (Sun and McDonough, 1989; Kelemen et al., 2004). CAOB—Central Asian orogenic belt.

the Hongguleneng ultramafic-mafic complex show a typical rifting trend due to their high TiO_2 contents (Fig. 9). (2) The Mayinebo gabbros and the Dasazi gabbros have Ti/V ratios of 28–33 and 47–57 (Fig. 12B), respectively, which are higher than that of basalts formed at arc settings (always <25) but similar to that of mid-ocean-

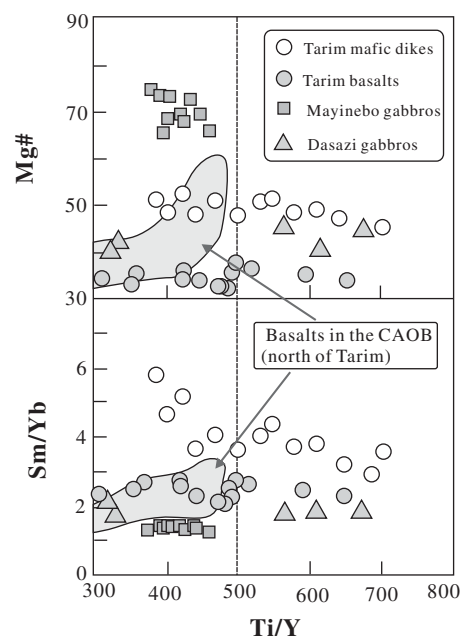


Figure 11. Diagram showing variation of Mg# and Sm/Yb against Ti/Y for Mayinebo gabbros and Dasazi gabbros. The mafic rocks in Tarim (data for Tarim mafic dikes and basalts are from Jiang et al., 2004a, 2004b) and the Central Asian orogenic belt (CAOB)(the gray area; data from D.W. Zhou et al., 2006) are also presented for comparison (see details in the text).

ridge basalt (MORB) and OIB (Shervais, 1982; Vermeesch, 2006). (3) The high TiO_2 contents of the Dasazi gabbros strongly argue against the case for a continental arc; on the contrary, their high TiO_2 , Zr, and total alkali contents, together with the characteristics of their incompatible elements ratios, suggest that OIB-like magma had been involved in their primitive magma. (4) The granodiorites from the Dasazi complex share some characteristics of A-type granites (e.g., high Zr contents and $10,000 \times \text{Ga}/\text{Al}$ ratios). (5) Granodiorites from both the Dasazi complex and the Chaergan granites have relatively high Rb and Nb + Y values, and they plot into the postorogenic or within-plate granite field (Fig. 12A) (Pearce et al., 1984).

ISOTOPIC AGE CONSTRAINTS ON VOLUMINOUS PERMIAN BASALTS, ULTRAMAFIC-MAFIC INTRUSIONS, AND A-TYPE GRANITES IN NORTHWESTERN CHINA

To better understand the petrogenesis and tectonic significance of the Permian magmatic rocks in northwestern China, we carried out a

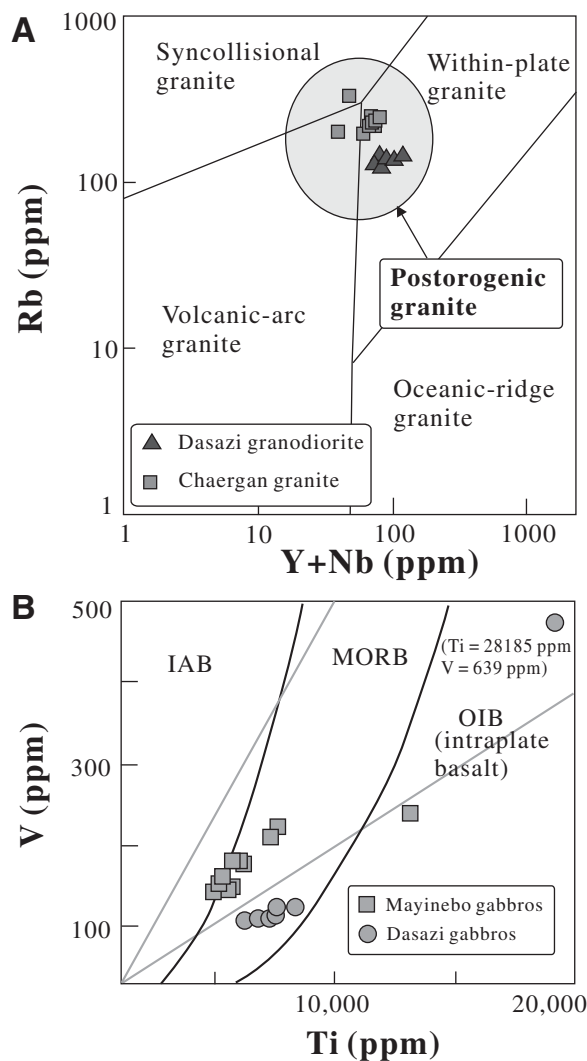


Figure 12. (A) Rb versus Nb + Y diagram showing that both the Dasazi granodiorites and the majority of the Chaergan granitic rocks plot into the post-orogenic area, indicating they were formed in an extensional setting (Pearce et al., 1984). (B) V versus Ti discrimination diagram for the Mayinebo and Dasazi gabbros. The black line is after Vermeesch (2006), and the gray line is after Shervais (1982). MORB—mid-ocean-ridge basalt; OIB—oceanic-island basalt.

regional data compilation. Figure 1 shows all Permian igneous rocks in the Tarim Basin, Tianshan, the Tuha Basin, the Santanghu Basin, the Junggar Basin, and the Altay ranges, marked with representative ages (see the full list of available ages in Table 4). Figure 13 shows the frequency distribution of known igneous ages from the region using ISOPLOT (Ludwig, 2001), highlighting peak activities at 275–270 Ma. Importantly, this period of igneous activity was characterized by voluminous mafic rocks rather than granites (Fig. 13; Table 4). A-type granites, including minor adakitic granites derived from mafic lower crust (Zhao et al., 2007), were emplaced at around the same time. In contrast, the older, 340–320 Ma magmatic peaks were dominated by granitic intrusions.

The most striking feature of the 275–270 Ma magmatism is the widespread occurrence of voluminous basalts in Tarim and surrounding regions (Figs. 1 and 14; Xinjiang B.G.M.R., 1993;

1999; Jiang et al., 2004a, 2004b; Jia et al., 2004; D.W. Zhou et al., 2006; Zhao et al., 2007), in addition to mafic-ultramafic intrusions and A-type granites. According to geophysical exploration and drill-hole data (Chen et al., 2006), the area covered by the Permian basalts (including minor related tuff and tuff-bearing rocks) preserved in the Tarim Basin, the Santanghu Basin, the Tuha Basin, and the Junggar Basin could reach up to 500,000 km² (Fig. 1). The thicknesses of the basaltic units vary between 100 and 1250 m (mostly >300 m; Fig. 14). Such a large volume of mafic magma would be difficult to generate by melting of the lithospheric mantle alone, which has been stable in a nonconvective state for a prolonged geological period.

Permian thermal events have also been identified elsewhere within the Central Asian orogenic belt, for example, the Weiya granite in Eastern Tianshan, which has a ⁴⁰Ar/³⁹Ar muscovite age of 269 Ma, and a biotite age of 281 Ma (Shu

et al., 2000). Along the southern margin of the Siberia craton, ⁴⁰Ar/³⁹Ar hornblende and biotite ages of 281–266 Ma (peak at ca. 275 Ma) are recorded (Buslov et al., 2004). Li et al. (1998) reported several liquid inclusion Rb–Sr isochron ages of ca. 275 Ma from quartz veins at the Xifengshan, Wangfeng, and Axi gold deposits. Recently, monazite chemical Th–U–total Pb isochron method (CHIME) ages of 260–270 Ma were obtained from high-temperature metamorphosed gneisses in the southern Altay Mountains (Zheng et al., 2007). These data not only suggest the occurrence of an intensive mafic igneous event, but also related hydrothermal activities.

DISCUSSIONS AND CONCLUSIONS

Bachu Large Igneous Province: Results of a ca. 275 Ma Plume Event in Northwestern China?

Syncollisional melt and postcollisional delamination in the Central Asian orogenic belt could properly explain the late Carboniferous (340–290 Ma) granitic rocks there and the minor mafic rocks dated at ca. 290 Ma north of Tianshan (Zhou et al., 2004; 340–290 Ma magmatic peaks in Fig. 13). Similar syn- to post-orogenic magmatism can be found in Mesozoic South China, where voluminous granites and minor mafic rocks occur (Li and Li, 2007), and the Mesozoic-Cenozoic granites in the Tibetan Plateau (Mo et al., 2006). However, it is unlikely that the delamination of subducted slab (slab break-off) could have induced the large volume of ca. 275–270 Ma mafic rocks in Tarim and the surrounding regions. Simple lithospheric extension or transtension also would have difficulties in explaining such a large-scale and voluminous outpouring of basaltic lavas.

Based on data and observations discussed here, we suggest that the coeval (275–270 Ma), voluminous, variably sourced mafic rocks in Tarim and surrounding regions, as well as the mafic intrusions and voluminous A-type granites in Tianshan, Altay, and even as far as Baikal and Mongolia (Pisarevsky et al., 2006; Izokh et al., 2009), constitute a Permian large igneous province in NW China and surrounding regions, which we term the Bachu large igneous province after C.L. Zhang et al. (2008). This large igneous province was most likely the product of a ca. 275 Ma mantle plume (e.g., Xia et al., 2004; Zhou et al., 2004; Pirajno et al., 2008; C.L. Zhang et al., 2008). This plume model would account for the bimodal but dominantly mafic nature of the 275–270 Ma magmatism, the synchronicity of the event over such a large regional extent (see section “Isotopic age constraints on voluminous Permian basalts, ultramafic-mafic

TABLE 4. AGE DATA OF THE PERMIAN IGNEOUS ROCKS IN TARIM AND SURROUNDING REGIONS

Tectonic unit	Locations	Rock type	Method	Age (Ma)	Reference	
Tarim Basin	Bachu BLIC	Pyroxene-bearing syenite	LA-ICP-MS (zircon)	275 ± 2	C.L. Zhang et al. (2008)	
	TC-3 DH	Basalt	Ar-Ar (WR)	273.5 ± 2.4	Jia et al. (1997)	
	TC-3 DH	Basalt	K-Ar (WR)	278 ± 2.3	Chen et al. (1997)	
	Bachu	Syenite dikes	SHRIMP (zircon)	277 ± 4	Yang et al. (2007)	
	Bachu	Mafic dikes	Sm-Nd (WR)	284 ± 15	Jiang et al. (2004a)	
Western Tienshan	Heishantou	Basalt	Ar-Ar (WR)	264 ± 5	Zhao et al. (2007)	
	Kezike	Basalt	Ar-Ar (WR)	288 ± 6	Zhao et al. (2007)	
	Zhaosu	Granite	Ar-Ar (Bi?)	285 ± 6	Zhao et al. (2003)	
	Sanchakou	Adakitic rocks	Rb-Sr (WR-M)	276 ± 4	Sun et al. (2002)	
	Sanchakou	Adakitic rocks	Rb-Sr (WR-M)	269 ± 17	Rui et al. (2004)	
	Variscan collision belt, Kyrgyzstan	A-type granite	Rb-Sr (WR-M)	269 ± 21	Solomovich and Trifonov (2002)	
		A-type granite	Rb-Sr (WR-M)	269 ± 8		
		A-type granite	Rb-Sr (WR-M)	273 ± 9		
		Yili granite	Biotite granite	Ar-Ar (Bi)	263.4 ± 0.6	DeJong et al. (2008)
		Baleigong granite	K-granite	SHRIMP (zircon)	272 ± 2	Wang et al. (2007a)
	Boluohuolu intrusive complex	Diorite		LA-ICP-MS (zircon)	301 ± 7	Wang et al. (2007b)
		Biotite granite			294 ± 7	
		K-granite			280 ± 5	
K-granite				266 ± 6		
K-granite				272 ± 6		
Eastern Tienshan	Hongliuhe UMC	Gabbro	SHRIMP (zircon)	272 ± 3	Han et al. (2006)	
	Pobei UMC	Gabbro	TIMS (zircon)	274 ± 4	Jiang et al. (2006)	
	Pobei UMC	Gabbro	SHRIMP (zircon)	278 ± 2	Li et al. (2006)	
	Huangshan UMC	Gabbro	SHRIMP (zircon)	271 ± 3	Zhou et al. (2004)	
	Huangshan UMC	Gabbro	SHRIMP (zircon)	274 ± 3	Han et al. (2004)	
	Sanchakou	Adakitic rocks	SHRIMP (zircon)	278 ± 4	Li et al. (2004)	
	Dashishan	Granite	SHRIMP (zircon)	273 ± 3	Qi et al. (2006)	
	Xifengshan	Biotite granite	Rb-Sr (WR)	284 ± 13	Li et al. (1998)	
	Xifengshan GD	Quartz vein	Rb-Sr (LI)	272 ± 3	Li et al. (1998)	
	Wangfeng GD	Quartz vein	Rb-Sr (LI)	277 ± 8.8	Li et al. (1998)	
	Axi GD	Quartz vein	Rb-Sr (LI)	275 ± 5	Li et al. (1998)	
	Yuxi SD	Granite	Rb-Sr (WR)	266.7 ± 4	Li et al. (1998)	
	Yuxi SD	Diorite	Rb-Sr (WR)	261 ± 8	Li et al. (1998)	
	Bole	Quartz porphyry	Ar-Ar (Bi?)	260 ± 5	Zhao et al. (2003)	
	Zhaosu	Granitic porphyry	Ar-Ar (Bi)	285 ± 6	Zhao et al. (2003)	
	Shawan	Basalt	Ar-Ar (WR)	277 ± 6	Zhao et al. (2003)	
	Zhongyangchang	Basalt	Ar-Ar (WR)	272 ± 5	Zhao et al. (2003)	
	Zhongyangchang	Basalt	Ar-Ar (WR)	263 ± 5	Zhao et al. (2003)	
	Bayinggou	Basalt	K-Ar (WR)	268 ± 4	No. 1 GP (1987)	
	Kangguer GD	Sericite schist	Ar-Ar (sericite)	267.6 ± 3.2	Li et al. (1998)	
	Kangguer GD	Quartz	Rb-Sr (LI)	282 ± 5	Li et al. (1998)	
	Shiyingtian GD	Granite	Rb-Sr (WR)	266 ± 3	Li et al. (1998)	
	Shiyingtian GD	Quartz vein	Rb-Sr (WR)	276 ± 7	Li et al. (1998)	
	Huoshibulake	A-type granite	TIMS (Zircon)	262 ± 3	Yang et al. (2001)	
	Konggure	Alkaline granites	TIMS (zircon)	265 ± 1.2	Jiang et al. (2001)	
	Poyi-Poshi	Ultramafic-mafic intrusion	SHRIMP	278 ± 2	Pirajno et al. (2008)	

(continued)

intrusions and A-type granites in NW China"; Fig. 13), the large volume and regional extent of the basaltic eruptions (Figs. 1 and 14), the petrogenetic characteristics of the mafic-ultramafic rocks, and the intraplate and anorogenic nature of the magmatism, some of which shows clear involvement of melts derived from the asthenospheric mantle (see sections "Petrogenesis" and "Tectonic implications").

Borisenko et al. (2006) and Yarmolyuk and Kozlovsky (2009) argued that some Permian Cu-Ni-(PGE) sulfide-bearing ultramafic-mafic intrusions in the Central Asian orogenic belt, e.g., the Kalatongke complex in southern Altai, were crystallized from picritic primitive magmas. Mass balance calculations also indicate that the layered intrusive complex in Huangshan area (Eastern Tienshan) was possibly crystallized from a picritic primitive magma

(MgO = 18%–24%; Zhou et al., 2004). As we mentioned already, though the rocks from the Hongguleneng complex are cumulates, the high Fo numbers of olivine suggest a possible picritic primitive magma of the complex. Importantly, as early as the 1970s, Vladimirov et al. (1979) had reported picritic porphyrites in the Zaisan area in eastern Kazakhstan. These integrated mineralogical, petrological, and geochemical data are all consistent with the presence of a Permian mantle plume with $T_p > 1350$ °C (McKenzie and Bickle, 1988). Nonetheless, such a plume model needs further verification. For instance, a plume model would predict pre- to synmagmatic crustal doming and denudation (e.g., Griffiths and Campbell, 1991; Li et al., 1999; He et al., 2003). Chen et al. (1997, 2006) indeed speculated about possible Early to mid-Permian crustal doming in Tarim based on

lithostratigraphic analyses, but further work is required to examine the precise timing and regional extent of such a doming event.

If the Bachu plume indeed existed, it would have occurred ~15 m.y. before the ca. 260 Ma Emeishan plume in southwestern China (e.g., Xu et al., 2001; He et al., 2007; Xu et al., 2008), and 25 m.y. before the 251 Ma Siberian Trap (plume) in Russia (e.g., Dobretsov, 2005). Such a sudden flare-up of plume activities in the Permian may represent the early stages of the Pangea superplume event, which is attributed to circum-Pangea subduction and mantle avalanches (Z.X. Li et al., 2004, 2008; Zhong et al., 2007; Li and Zhong, 2009).

The Central Asian orogenic belt was one of the most important sites of juvenile crustal growth during the Phanerozoic (e.g., Jahn et al., 2004). Permian mafic-ultramafic intrusions and

TABLE 4. AGE DATA OF THE PERMIAN IGNEOUS ROCKS IN TARIM AND SURROUNDING REGIONS (continued)

Tectonic unit	Locations	Rock type	Method	Age (Ma)	Reference
Tuha Basin	Zhaobishan	Basalt	Ar-Ar (WR)	273 ± 1	D.W. Zhou et al. (2006)
	Zhaobishan	Basalt	Ar-Ar (WR)	276 ± 2	D.W. Zhou et al. (2006)
	Cheguluquan	Basalt	Ar-Ar (WR)	270 ± 1	D.W. Zhou et al. (2006)
	Kula	Basalt	Ar-Ar (WR)	269 ± 1	D.W. Zhou et al. (2006)
	Kula	Basalt	Ar-Ar (WR)	276 ± 1	D.W. Zhou et al. (2006)
	Dananhu	Alkaline basalt	Ar-Ar (WR)	270 ± 1	D.W. Zhou et al. (2006)
	Y-1 DH	Basalt	Ar-Ar (WR)	278 ± 1	D.W. Zhou et al. (2006)
	L-1 DH	Basalt	Ar-Ar (WR)	281 ± 1	D.W. Zhou et al. (2006)
Santanghu Basin	Shacan-1 DH	Basalt	Ar-Ar (WR)	290 ± 1	D.W. Zhou et al. (2006)
	M8-02 DH	Basalt	Ar-Ar (WR)	266 ± 0.54	D.W. Zhou et al. (2006)
	Tc1-01 DH	Basalt	Ar-Ar (WR)	273 ± 0.35	D.W. Zhou et al. (2006)
	Tc2-02 DH	Basalt	Ar-Ar (WR)	273 ± 0.46	D.W. Zhou et al. (2006)
	T4-01 DH	Basalt	Ar-Ar (WR)	266 ± 0.56	D.W. Zhou et al. (2006)
	Habahe county	Granite	Ar-Ar(hornblende)	267 ± 4	Yuan et al. (2007)
Jungger Basin	Jimunai	Basalt	Sm-Nd (WR)	281 ± 24	Zhou (personal commun.)
	Western Jungger	K-granite	SHRIMP (zircon)	276 ± 5	Han et al. (2006)
	Western Jungger	Rhyolite	SHRIMP (zircon)	271 ± 6.5	Liu et al. (2005)
	Kelamayi City	Mafic dike	K-Ar (WR)	265.5 ± 5.4	Li et al. (2004)
		Mafic dike	K-Ar (WR)	265.5 ± 7.7	
		Mafic dike	K-Ar (WR)	271.5 ± 8.1	
		Mafic dike	K-Ar (WR)	270.2 ± 8.1	
		Mafic dike	K-Ar (WR)	267.1 ± 8	
	Eastern Juggar	Diorite	Rb-Sr (WR-M)	274 ± 5	Chen et al. (2004)
	Eastern Juggar	A-type granite	Rb-Sr (WR-M)e	281 ± 6	Chen et al. (2004)
	Eastern Juggar	A-type granite	Rb-Sr (WR-M)	278 ± 6	Chen et al. (2004)
South of Altay	Hongguleneng	UMC	SHRIMP (zircon)	273.2 ± 2.6	This study
	Dasazi BMC	Gabbro	SHRIMP (zircon)	269.4 ± 2.5	This study
	Mayinebo gabbros	Gabbro	SHRIMP (zircon)	272.5 ± 2.4	This study
	Chaergan	Granite	SHRIMP (zircon)	277 ± 3.2	This study
	Fuyun	A-type granite	SHRIMP (zircon)	273 ± 6	Han et al. (2006)
	Fuyun	A-type granite	SHRIMP (zircon)	275 ± 4	Tong et al. (2006)
	Chonghuer MMR	Gneiss	CHIME(monazite)	268 ± 10	Zheng et al. (2007)
	Taerlang MMR	Gneiss	CHIME(monazite)	261 ± 20	Zheng et al. (2007)
	Altay city	A-type granite	SHRIMP (zircon)	276 ± 9	Wang et al. (2005)
	Altay city	Silicic dikes	SHRIMP (zircon)	277 ± 10	Gong et al. (2007)
	Dasazi	Granite	Rb-Sr (WR)	274 ± 12	No. 2 Geological Party, BGMR (1998, unpublished)
		(mingled with the Dasazi gabbro)			Izokh et al. (2009)
	Dzara-Ula (Mongolia)	Monzogabbro	SHRIMP (zircon)	269.2±4.1	
	Southern Siberia	Baikal area	Mafic dike	SHRIMP (zircon)	275 ± 4

Note: GD—gold deposits; SD—silver deposits; LI—fluid inclusion; Bi—biotite; WR—whole rock; DH—drill hole; UMC—ultramafic-mafic intrusive complex; BMC—bimodal intrusive complex.

A-type granites in the Central Asian orogenic belt (e.g., Han et al., 1999) were important parts of this episode of crustal growth. If the plume model as proposed here is correct, it would suggest that mantle plume activity made major contributions to crustal growth in the Central Asian orogenic belt.

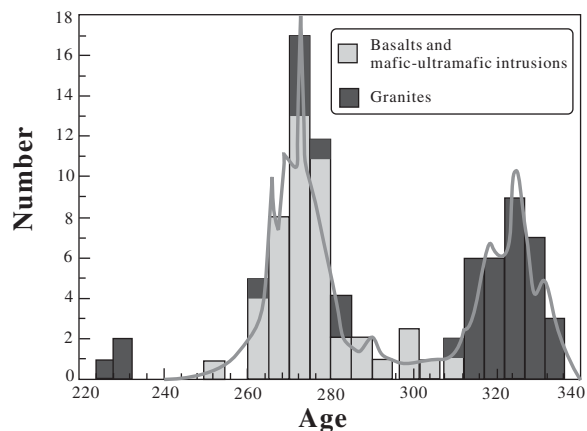
Two Distinct Mantle Domains in Northwestern China?

We notice that the elemental and isotopic compositions of the Permian-Carboniferous mafic rocks are quite different between Tarim and those further to the north (Tianshan, the Tuha Basin, the Santanghu Basin, the Junggar Basin, and the Altay) (Fig. 8). The basalts in Tarim (samples from the Keping area and several drill holes in Tarim) are characterized by a tholeiitic trend (Jiang et al., 2004b; Yang et al., 1995; Fig. 6), low Mg # (25–38), high Ti ($TiO_2 = 2.7\text{--}5.3$ wt%, $Ti/Y = 300\text{--}650$, mostly above 500) (high-Ti type; Fig. 11), Zr (280–

470 ppm), total REE (156–250 ppm) contents, enriched LREEs ($La_N/Yb_N \oplus 6.5$), negative $\epsilon_{Nd}(t)$ (–3.1 to –1.5), and high ($^{87}Sr/^{86}Sr$) ratios (Fig. 8). On the other hand, they have high Nb/La (0.8–1.2, mostly above 1.0), Nb/U (>25), and Nb/Th (>3.5) ratios, excluding the pos-

sibility of the crustal contamination leading to the isotopic enrichment (Fig. 10). The variable negative Sr anomaly ($\delta Sr = Sr_N/[Ce_N \times Nd_N]^{1/2} = 0.3\text{--}0.7$) in the basalt could reflect high Eu^{3+}/Eu^{2+} ratios in the magmas because of the absence of negative Eu anomalies ($\delta Eu \oplus 1.0$)

Figure 13. Cumulative age spectra of the Permian igneous rocks in Tarim and the Central Asian orogenic belt. The age data and references are listed in Table 4.



(Frey et al., 1993; Xia et al., 2004). All of these characteristics strongly argue for partial melting of a long-term enriched lithospheric mantle source. Moreover, as the REE and HFSE ratios are closely related with temperature-pressure conditions, and the degree of partial melting remained constant during crystal fractionation, the least contaminated basalt samples (samples with Nb/La > 1.0) in Tarim have relatively stable La/Sm (3–5), Sm/Yb (2–2.7), Ce/Y (1.1–1.6), and Zr/Nb (8–10) values, indicating that their primitive magma was derived from 5% to 15% partial melting within the spinel-garnet stability field, corresponding to the depth of 60–80 km (McKenzie and Bickle, 1988). The Permian mafic dikes and ultramafic-mafic-syenite complex in Tarim, as we have suggested previously (C.L. Zhang et al., 2008), were crystallized from an OIB-like basaltic magma derived from partial melting of an asthenospheric mantle source, according to their high alkali contents, positive $\epsilon_{Nd}(t)$ (1.5–5.7), relatively low ($^{87}Sr/^{86}Sr$)_i (Sr isotope compositions could have been altered during hydrothermal alteration process; Fig. 8), and high Ti/Y (high-Ti type; Fig. 11), Nb/La (1.0–1.2), Nb/U, and Nb/Th ratios (Fig. 10). Thus, we suggest that the asthenosphere-derived magma could have supplied the heat required to melt the lower lithospheric mantle (60–80 km).

The basalts and ultramafic-mafic intrusions (mafic dikes included) in Tianshan and north of Tianshan (the Tuha, Santanghu, Junggar Basins) exhibit systematic tholeiitic trends (Fig. 6), having low TiO₂ (mostly less than 2.0 wt%) and Ti/Y ratios (less than 500, low-Ti type; Fig. 11), enriched LILE and LREEs, low Nb/La (mostly less than 0.5), Nb/U, and Nb/Th ratios (Fig. 10), and variable initial Nd and Sr values ($\epsilon_{Nd}(t) = 0-9.3$, [$^{87}Sr/^{86}Sr$]_i = 0.702–0.7085). On the $\epsilon_{Nd}(t)$ versus ($^{87}Sr/^{86}Sr$)_i diagram (Fig. 8), all the samples plot between the depleted mantle (DM) and II-type enriched (EMII-type) mantle sources. Thus, these mafic rocks were most likely derived from a depleted mantle source metasomatized by subducting slabs (Zhou et al., 2004). We noticed that the basalts from Eastern Tianshan have relatively higher Nb/La ratios (0.4–0.7) and $\epsilon_{Nd}(t)$ values, slightly elevated Th_N/Nb_N (greater than 1.0), and lower La_N/Yb_N ratios (1–8, mostly <3.0) than those of the other basalts in Western Tianshan and the three basins north of Tianshan (i.e., the Tuha, Santanghu, and Junggar Basins) (Zhao et al., 2006, 2007); these features suggest that they were derived from partial melting of a depleted continental lithospheric mantle that had only been slightly affected by metasomatism of subducting slabs (Saunders et al., 1992).

Geochemical and Sm-Nd isotopic data indicate that large proportions of the late Paleozoic

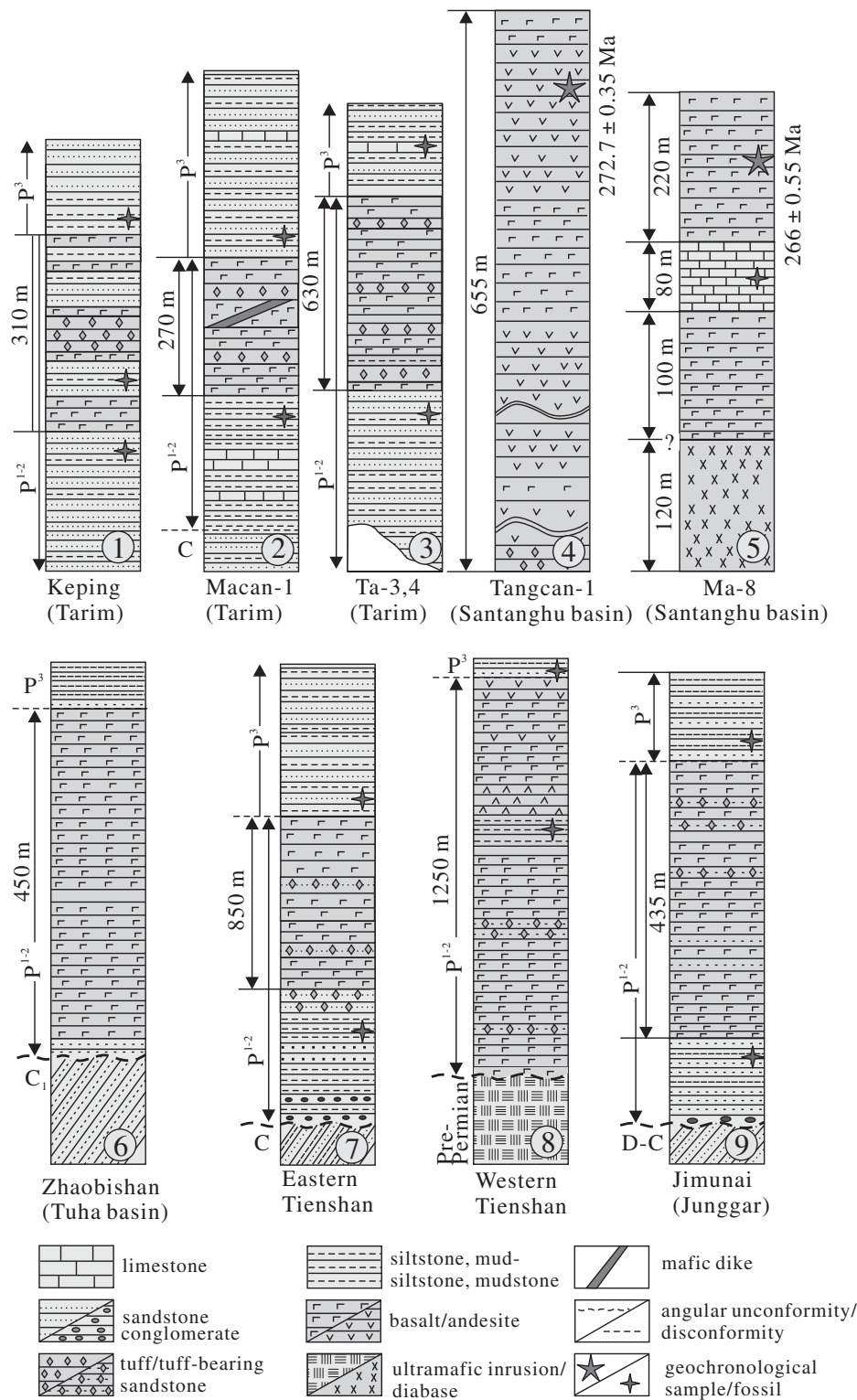


Figure 14. Stratigraphic positions and thicknesses of the Permian basalts in the Tarim, Tianshan, Santanghu, Tuha, and Junggar Basins (data sources: Xinjiang B.G.M.R., 1999; Jiang et al., 2004b; Jia et al., 2004; D.W. Zhou et al., 2006).

granites in the Central Asian orogenic belt were A-type magmas with positive ϵ_{Nd} values, indicating a juvenile character and suggesting a direct or indirect role (more likely) for mantle magmatism in their formation (Han et al., 1999; Jahn et al., 2004; Chen and Jahn, 2004). Modeling calculations indicate that ~1%–5% basaltic magma from the mantle had been added into the silicic magma derived from partial melting of the juvenile mafic crust. This is evidenced by the pervasive mafic inclusions mingled in the A-type granites.

Based on the analyses herein, we can divide the Permian basalts and ultramafic-mafic intrusions on the basis of their geochemical characteristics. They appear to have been derived from two separate mantle domains, i.e., the Tarim domain and the Central Asian orogenic belt domain (Fig. 1). The Tarim domain is a long-term enriched continental lithospheric mantle that had not been metasomatized by Phanerozoic subducted materials, while the Central Asian orogenic belt mantle is intensively depleted and variably enriched by the Phanerozoic subduction slab-derived fluid and/or subducted sediments.

ACKNOWLEDGMENTS

We thank W. Pu and T. Yang for helping with major and trace elements and Sr-Nd isotope analyses, and Q. T. Zeng, and H. Tao for assistance with sensitive high-resolution ion microprobe (SHRIMP) data acquisition. We also thank R. Ernst, A.S. Borisenko, A.E. Izokh, and an anonymous reviewer for their constructive reviews of the manuscript. This work was supported by National Science Foundation of China (grants 40721063, 40772123, and 40728002), Chinese Academy of Sciences SAFEA International Partnership Program for Creative Research Teams, and Australian Research Council (DP0770228). This is a TIGER publication.

REFERENCES CITED

- Bai, W.J., and Zhou, M.F., 1988, Variation in chemical composition of chrome spinels from Hongguleneng ophiolite, Xinjiang, and their significance: *Acta Mineralogica Sinica*, v. 8, p. 313–323.
- Bai, W.J., and Zhou, M.F., 1989, Study on the chemical compositions of the pyroxene in the Hongguleneng ophiolite, Xinjiang: *Geology Review*, v. 35, p. 107–118.
- Bai, W.J., and Zhou, M.F., 1991, Geochemical characteristics and origin of the cumulates of the Hongguleneng ophiolite, Xinjiang: *Bulletin of the Chinese Academy of Geological Sciences*, v. 24, p. 63–78.
- Barbarin, B., 1996, Genesis of the two main types of peraluminous granitoids: *Geology*, v. 24, p. 295–298, doi: 10.1130/0091-7613(1996)024<0295:GOTTMT>2.3.CO;2.
- Barbarin, B., 1999, A review of the relationships between granitoid types, their origins and their geodynamic environments: *Lithos*, v. 46, p. 605–626, doi: 10.1016/S0024-4937(98)00085-1.
- Borg, L.E., and Clyne, M.A., 1998, The petrogenesis of felsic calcalkaline magmas from the southernmost Cascades, California: Origin by partial melting of basaltic lower crust: *Journal of Petrology*, v. 39, p. 1197–1222, doi: 10.1093/petrology/39.6.1197.
- Borisenko, A.S., Sotnikov, V.I., Izokh, A.E., Polyakov, G.V., and Obolensky, A.A., 2006, Permo-Triassic mineralization in Asia and its relation to plume magmatism: *Russian Geology and Geophysics*, v. 47, p. 166–182.
- Buslov, M.M., Watanabe, T., Fujiwara, Y., Iwata, K., Smirnova, L.V., Safonov, I.Y., Semakov, N.N., and Kiryanov, A.P., 2004, Late Paleozoic faults of the Altai region, Central Asia: Tectonic pattern and model of formation: *Journal of Asian Earth Sciences*, v. 23, p. 655–671, doi: 10.1016/S1367-9120(03)00131-7.
- Chen, B., and Jahn, B.M., 2004, Genesis of post-collisional granitoids and basement nature of the Junggar terrane, NW China: Nd-Sr isotope and trace element evidence: *Journal of Asian Earth Sciences*, v. 23, p. 691–703, doi: 10.1016/S1367-9120(03)00118-4.
- Chen, H.L., Yang, S.F., and Dong, C.W., 1997, The discovery of Early Permian basic rock belt in Tarim Basin and its tectonic meanings: *Geochimica*, v. 22, p. 77–87.
- Chen, H.L., Yang, S.F., Wang, Q.H., Luo, J.C., Jia, C.Z., Wei, G.Q., and Li, Z.L., 2006, Sedimentary response to the Early-Mid Permian basaltism in the Tarim plate: *Geology in China*, v. 33, p. 545–552.
- Cox, K.G., Bell, J.D., and Pankhurst, R.J., 1979, *The Interpretation of Igneous Rocks*: London, Allen and Unwin, 450 p.
- DeJong, K., Wang, B., Faure, M., Shu, L.S., Cluzel, D., Charvet, J., Ruffet, G., and Chen, Y., 2008, New $^{40}\text{Ar}/^{39}\text{Ar}$ age constraints on the late Palaeozoic tectonic evolution of the Western Tianshan (Xinjiang, northwestern China), with emphasis on Permian fluid ingress: *International Journal of Earth Sciences*, v. 98, p. 1239–1258.
- Dobretsov, N.L., 2005, 250 Ma large igneous provinces of Asia: Siberian and Emeishan Traps (plateau basalts) and associated granitoids: *Russian Geology and Geophysics*, v. 46, p. 870–890.
- Frey, F.A., Garcia, M.O., Wise, W.S., Kennedy, A., Gurriet, P., and Albarede, F., 1993, The evolution of Mauna Kea volcano, Hawaii: Petrogenesis of tholeiitic and alkali basalts: *Journal of Geophysical Research*, v. 98, p. 14,347–14,375.
- Gerdes, A., Montero, P., Bea, F., and Fershter, G., 2002, Peraluminous granites frequently with mantle-like isotope compositions: The continental-type Murzinka and Dzhabyk batholiths of the eastern Urals: *International Journal of Earth Sciences*, v. 91, p. 3–19, doi: 10.1007/s005310100195.
- Gong, H.L., Chen, Z.L., Hu, Y.Q., Li, L., Lai, X.R., Ma, Q.Y., Li, Y.Y., Hu, B., and Zhang, W.G., 2007, Geochemical characteristics of acidic dike swarm from the eastern segment of the Ertis tectonic belt, Altai orogeny and its geological implications: *Acta Petrologica Sinica*, v. 23, p. 889–899.
- Griffiths, R.W., and Campbell, I.H., 1991, On the dynamics of long-lived plume conduits in the convecting mantle: *Earth and Planetary Science Letters*, v. 103, p. 214–227, doi: 10.1016/0012-821X(91)90162-B.
- Han, B.F., He, G.Q., and Wang, S.G., 1999, Postcollisional mantle-derived magmatism, underplating and implication for the basement of the Junggar Basin: *Sciences in China*, ser. D, v. 42, p. 113–119.
- Han, B.F., Ji, J.Q., Song, B., Chen, L.H., and Li, Z.H., 2004, Zircon SHRIMP U-Pb ages of the Kalatongke and Huangshandong Cu-Ni-bearing ultramafic-mafic intrusions and their geological significances: *Chinese Science Bulletin*, v. 49, p. 2324–2328.
- Han, B.F., Ji, J.Q., Song, B., Chen, L.H., and Zhang, L., 2006, Late Paleozoic vertical growth of continental crust around the Junggar Basin, Xinjiang, China (Part I): Timing of post-collisional plutonism: *Acta Petrologica Sinica*, v. 22, p. 1077–1086.
- He, B., Xu, Y.G., Chung, S.L., Xiao, L., and Wang, Y.M., 2003, Sedimentary evidence for a rapid, kilometer-scale crustal doming prior to the eruption of the Emeishan flood basalts: *Earth and Planetary Science Letters*, v. 213, p. 391–405, doi: 10.1016/S0012-821X(03)00323-6.
- He, B., Xu, Y.G., Huang, X.L., Luo, Z.Y., Shi, Y.R., Yang, Q.J., and Yu, S.Y., 2007, Age and duration of the Emeishan flood volcanism, SW China: *Geochemistry and SHRIMP zircon U-Pb dating of silicic ignimbrites, post-volcanic Xuanwei Formation and clay tuff at the Chaotian section*: *Earth and Planetary Science Letters*, v. 255, p. 306–323, doi: 10.1016/j.epsl.2006.12.021.
- Huang, J.H., Jin, Z.D., and Li, F.C., 1999, Age determination and Sm-Nd isotopic composition of the Hongguleneng ophiolite, Xinjiang: *Chinese Science Bulletin*, v. 44, p. 1004–1007.
- Jahn, B.M., Windley, B., Natal'in, B., and Dobretsov, N., 2004, Phanerozoic continental growth in Central Asia: *Journal of Asian Earth Sciences*, v. 23, p. 599–603, doi: 10.1016/S1367-9120(03)00124-X.
- Jia, C.Z., 1997, *Tectonic characteristics and oil gas of the Tarim Basin, China*: Beijing, Petroleum Industry Press, p. 23–45 (in Chinese).
- Jia, C.Z., Zhang, S.B., and Wu, S.Z., 2004, *Stratigraphy of the Tarim Basin and Adjacent Areas, Volume 2*: Beijing, Science Press, 513 p.
- Jiang, C.Y., Wu, W.K., Li, L.C., Mu, Y.M., Bai, K.Y., and Zhao, X.L., 2001, *Tectonic Evolution of the Eastern Part of the Southern Tianshan*: Beijing, Geological Publishing House, 160 p. (in Chinese).
- Jiang, C.Y., Jia, C.Z., Li, L.C., Zhang, P.B., Lu, D.R., and Bai, K.Y., 2004a, Source of the Fe-enriched-type high-Mg magma in Mazhartag region: Xinjiang: *Acta Geologica Sinica*, v. 78, p. 770–780.
- Jiang, C.Y., Zhang, P.B., Lu, D.R., Bai, K.Y., Wang, Y.P., Tang, S.H., Wang, J.H., and Yang, C., 2004b, Petrology, geochemistry and petrogenesis of the Kalpin basalts and their Nd, Sr and Pb isotopic compositions: *Geological Review*, v. 50, p. 492–500.
- Jiang, C.Y., Cheng, S.L., Ye, S.F., Xia, M.Z., Jiang, H.B., and Dai, Y.C., 2006, Litho-geochemistry and petrogenesis of Zhongposhan mafic rock body, at Beishan region, Xinjiang: *Acta Geologica Sinica*, v. 22, p. 115–126.
- Kelemen, P.B., Hanghoj, K., and Greene, A.R., 2004, One view of the geochemistry of subduction-related magmatic arcs, with an emphasis on primitive andesite and lower crust, *in* Rudnick, R.L., ed., *Treatise on Geochemistry*, Volume 3: Amsterdam, Elsevier—Oxford, Pergamon, p. 593–659.
- Li, H.Q., Xie, C.F., Chang, H.L., Cai, H., Zhu, J.P., and Zhou, S., 1998, Study on the Metallogenetic Chronology of Nonferrous and Precious Metallic Ore Deposits in North Xinjiang, China: Beijing, Geological Publishing House, 250 p. (in Chinese with English abstract).
- Li, H.Q., Chen, F.W., Lu, Y.F., Yang, H.M., Guo, J., and Mei, Y.P., 2004, Zircon SHRIMP U-Pb age and strontium isotope of mineralized granitoids in the Sanchakou copper polymetallic deposit: East Tianshan Mountains: *Acta Geoscientia Sinica*, v. 25, p. 191–195.
- Li, H.Q., Chen, F.W., Mei, Y.P., Wu, H., Chen, S.L., and Dai, Y.C., 2006, Isotopic ages of No. 1 intrusive body in Pobei mafic-ultramafic belt of Xinjiang and their geological significance: *Acta Metallogica Sinica*, v. 25, p. 464–469.
- Li, J.Y., 2006, Permian geodynamic setting of Northeast China and adjacent regions: Closure of the paleo-Asian Ocean and subduction of the paleo-Pacific plate: *Journal of Asian Earth Sciences*, v. 26, p. 207–224, doi: 10.1016/j.jseas.2005.09.001.
- Li, X.H., Sun, M., Wei, G.-J., Liu, Y., Lee, C.Y., and Malpas, J.G., 2000, Geochemical and Sm-Nd isotopic study of amphibolites in the Cathaysia block, SE China: Evidence for extremely depleted mantle in the Paleoproterozoic: *Precambrian Research*, v. 102, p. 251–262, doi: 10.1016/S0301-9268(00)00067-X.
- Li, X.H., Li, Z.X., Wingate, M.T.D., Chung, S.L., Liu, Y., Lin, G.C., and Li, W.X., 2006, Geochemistry of the 755 Ma Mundine Well dyke swarm, northwestern Australia: Part of a Neoproterozoic mantle superplume beneath Rodinia?: *Precambrian Research*, v. 146, p. 1–15, doi: 10.1016/j.precamres.2005.12.007.
- Li, X.Z., Han, B.F., Ji, J.Q., Li, Z.H., Liu, Z.Q., and Yang, B., 2004, Geology, geochemistry and K-Ar ages of the Karamay basic-intermediate dyke swarm from Kelamayi of Xinjiang, China: *Geochimica*, v. 33, p. 574–584.
- Li, Z.X., and Li, X.H., 2007, Formation of the 1300-km-wide intracontinental orogen and postorogenic magmatic province in Mesozoic South China: A flat-slab subduction model: *Geology*, v. 35, p. 179–182, doi: 10.1130/G23193A.1.
- Li, Z.X., and Zhong, S., 2009, Supercontinent–superplume coupling, true polar wander and plume mobility: Plate dominance in whole-mantle tectonics: *Physics of the*

- Earth and Planetary Interiors, v. 176, p. 143–156, doi: 10.1016/j.pepi.2009.05.004.
- Li, Z.X., Li, X.H., Kinny, P.D., and Wang, J., 1999, The breakup of Rodinia: Did it start with a mantle plume beneath South China?: Earth and Planetary Science Letters, v. 173, p. 171–181, doi: 10.1016/S0012-821X(99)00240-X.
- Li, Z.X., Bogdanova, S.V., Collins, A.S., Davidson, A., De Waele, B., Ernst, R.E., Fitzsimons, I.C.W., Fuck, R.A., Gladkochub, D.P., Jacobs, J., Karlstrom, K.E., Lu, S., Natapov, L.M., Pease, V., Pisarevsky, S.A., Thrane, K., and Vernikovsky, V., 2008, Assembly, configuration, and break-up history of Rodinia: A synthesis: Precambrian Research, v. 160, p. 179–210, doi: 10.1016/j.precamres.2007.04.021.
- Liu, Z.Q., Han, B.F., and Ji, J.Q., 2005, Age and geochemistry of the post-collisional granitic rocks from eastern Alataw Mountains, Xinjiang, and implication for vertical continental growth: Acta Petrologica Sinica, v. 21, p. 623–639.
- Loucks, R.R., 1990, Discrimination of ophiolitic from non-ophiolitic ultramafic-mafic allochthons in orogenic belts by the Al/Ti ratios in clinopyroxene: Geology, v. 18, p. 346–349, doi: 10.1130/0091-7613(1990)018<0346:DOOFNU>2.3.CO;2.
- Ludwig, K.R., 1999, Using Isoplot/EX, Version 2; a Geochemical Toolkit for Microsoft Excel: Berkeley Geochronological Center Special Publication 1a, 47 p.
- Ludwig, K.R., 2001, Squid 1.02: A User's Manual: Berkeley Geochronological Center Special Publication 2, 19 p.
- Maniar, P.D., and Piccoli, P.M., 1989, Tectonic discrimination of granitoids: Geological Society of America Bulletin, v. 101, p. 635–643, doi: 10.1130/0016-7606(1989)101<0635:TDOG>2.3.CO;2.
- McKenzie, D.P., and Bickle, M.J., 1988, The volume and composition of melt generated by extension of the lithosphere: Journal of Petrology, v. 29, p. 625–679.
- Mo, X.X., Zhao, Z.D., Deng, J.F., Martin, F., Yu, X.H., Luo, Z.H., Li, Y.G., Zhou, S., Dong, G.C., Zhu, D.C., and Wang, L., 2006, Petrology and geochemistry of post-collisional volcanic rocks from the Tibetan Plateau: Implications for lithosphere heterogeneity and collision-induced asthenospheric mantle flow, in Dilek, Y., and Pavlides, S., ed., Postcollisional Tectonics and Magmatism in the Mediterranean Region and Asia: Geological Society of America Special Paper 409, p. 507–530.
- Montel, L.M., and Vielzeuf, D., 1997, Partial melting of metagreywackes: Part II. Compositions of minerals and melts: Contributions to Mineralogy and Petrology, v. 128, p. 176–196, doi: 10.1007/s004100050302.
- No. 1 Geological Party, Xinjiang Bureau of Geology and Mineral Resources (BGMR), 1987, Assemblage of data of isotope geological ages, Xinjiang: Xinjiang Geology, v. 5, p. 16–106 (in Chinese with English abstract).
- No. 2 Geological Party, Xinjiang BGMR, 1998, Geological report of the 1/50000 geological mapping of the Dasazi area: Xinjiang, China, Xinjiang BGMR, p. 122–160 (in Chinese).
- Pearce, J.A., and Cann, J.R., 1973, Tectonic setting of basic volcanic rocks determined using trace elements analysis: Earth and Planetary Science Letters, v. 19, p. 290–300, doi: 10.1016/0012-821X(73)90129-5.
- Pearce, J.A., Harris, N.B.W., and Tindle, A.G., 1984, Trace element discrimination diagrams for the tectonic interpretation of granitic rocks: Journal of Petrology, v. 25, p. 956–983.
- Peng, Y.G., Bao, P.S., Wang, X.B., and Hao, Z.G., 1991, Origin of Pl-lherzolite in the Hongluneng ophiolite, Xinjiang: Acta Petrologica et Mineralogica, v. 10, p. 114–125.
- Petcovic, H.L., and Grunder, A.L., 2003, Texture and thermal history of partial melting in tonalitic country rock at the margin of a basalt dike, Wallowa Mountains, Oregon: Journal of Petrology, v. 44, p. 2287–2312, doi: 10.1093/petrology/egg078.
- Pirajno, F., Mao, J.W., Zhang, Z.C., Zhang, Z.H., and Chai, F.M., 2008, The association of mafic-ultramafic intrusions and A-type magmatism in the Tian Shan and Altai orogens, NW China: Implications for geodynamic evolution and potential for the discovery of new ore deposits: Journal of Asian Earth Sciences, v. 32, p. 165–183.
- Pisarevsky, S.A., Gladkochub, D.P., Donskaya, T.A., Waele, B.D., and Mazukabzov, A.M., 2006, Palaeomagnetism and geochronology of mafic dykes in south Siberia, Russia: The first precisely dated Early Permian palaeomagnetic pole from the Siberian craton: Geophysical Journal International, v. 167, p. 649–658, doi: 10.1111/j.1365-246X.2006.03160.x.
- Rapp, R.B., and Watson, E.B., 1995, Dehydration of metabasalt at 8–32 kbar: Implications for continental growth and crustal-mantle recycling: Journal of Petrology, v. 36, p. 891–931.
- Roeder, P.L., and Emsile, R.F., 1970, Olivine-liquid equilibrium: Contributions to Mineralogy and Petrology, v. 29, p. 275–289, doi: 10.1007/BF00371276.
- Rudnick, R.L., and Gao, S., 2003, Composition of the continental crust, in Rudnick, R.L., ed., Treatise on Geochemistry, Volume 3: Amsterdam, Elsevier—Oxford, Pergamon, p. 1–64.
- Rui, Z.Y., Zhang, L.S., Chen, Z.Y., Wang, L.S., Liu, Y.L., and Wang, Y.T., 2004, Discussion on the magma sources and the mother rocks of the porphyritic copper deposits: Acta Petrologica Sinica, v. 20, p. 229–238.
- Saunders, A.D., Storey, M., Kent, R.W., and Norry, M.J., 1992, Consequences of plume-lithosphere interaction, in Storey, B.C., Alabaster, T., and Pankhurst, R.J., eds., Magmatism and the Cause of Continental Breakup: Geological Society of London Special Publication 68, p. 41–60.
- Sengör, A.M.C., Natalin, B.A., and Burtman, V.S., 1993, Evolution of the Altaid tectonic collage and Palaeozoic crustal growth in Eurasia: Nature, v. 364, p. 299–307, doi: 10.1038/364299a0.
- Shervais, J.W., 1982, Ti-V plots and the petrogenesis of modern and ophiolitic lavas: Earth and Planetary Science Letters, v. 59, p. 101–118, doi: 10.1016/0012-821X(82)90120-0.
- Shu, L.S., Chen, Y., Lu, H., Charvet, J., Laurent, S., and Yin, D., 2000, Paleozoic accretionary terranes in northern Tianshan: NW China: Chinese Journal of Geochemistry, v. 19, p. 193–202, doi: 10.1007/BF03166877.
- Sisson, T.W., Ratajeski, K., and Hankins, W.B., 2005, Volcanic granitic magmas from common basaltic sources: Contributions to Mineralogy and Petrology, v. 148, p. 635–661, doi: 10.1007/s00410-004-0632-9.
- Solomovich, L.I., and Trifonov, B.A., 2002, Postcollisional granites in south Tien Shan Variscan collisional belt, Kyrgyzstan: Journal of Asian Earth Sciences, v. 21, p. 7–21, doi: 10.1016/S1367-9120(02)00008-1.
- Stacey, J.S., and Kramers, J.D., 1975, Approximation of terrestrial lead isotope evolution by two-stage model: Earth and Planetary Science Letters, v. 26, p. 207–221, doi: 10.1016/0012-821X(75)90088-6.
- Sun, M., Yuan, C., Xiao, W., Long, X., Xia, X., Zhao, G., Lin, S., Wu, F., and Kröner, A., 2008, Zircon U-Pb and Hf isotopic study of gneissic rocks from the Chinese Altai: Progressive accretionary history in the early to middle Paleozoic: Chemical Geology, v. 247, p. 352–383, doi: 10.1016/j.chemgeo.2007.10.026.
- Sun, S.S., and McDonough, W.F., 1989, Chemical and isotopic systematics of oceanic basalt: Implication for mantle composition and processes, in Saunders, A.D., and Norry, M.J., eds., Magmatism in the Ocean Basin: Geological Society of London Special Publication 42, p. 528–548.
- Sun, Y., Tang, J.X., and Mu, J.L., 2002, Geochemistry and metallogenesis of the Sanchakou copper deposit: Acta Metallogica Sinica, v. 21, supplement, p. 459–462 (in Chinese with English abstract).
- Tang, H.F., Su, Y.P., Liu, C.Q., Hou, G.S., and Wang, Y.B., 2007, Zircon U-Pb age of the plagiogranite in Kalamaili belt, northern Xinjiang, and its tectonic implications: Geotectonica et Metallogenia, v. 31, p. 110–117.
- Tong, Y., Wang, T., Kovach, V.P., Hong, D.W., and Han, B.F., 2006, Age and origin of the Takeshiken postorogenic alkali-rich intrusive rocks in Southern Altai, near the Mongolian boarder of China and its implications for continental growth: Acta Petrologica Sinica, v. 22, p. 1267–1278.
- Vermeesch, P., 2006, Tectonic discrimination diagrams revisited: Geochemistry, Geophysics, Geosystems, v. 7, p. Q06017, doi: 10.1029/2005GC001092.
- Vladimirov, A.G., Izokh, A.E., and Yakovleva, N.A., 1979, Pycritic porphyrites of the Zaisan fold area and their genesis: Dokl AS USSR, v. 247, p. 1236–1241.
- Wang, B., Shu, L.S., Cluzel, D., Faure, M., and Charvet, J., 2007a, Geochronological and geochemical studies on the Borohoro plutons, north of Yili, NW Tianshan, and their tectonic implication: Acta Geologica Sinica, v. 23, p. 1885–1900.
- Wang, C., Liu, L., Luo, J.H., Che, Z.C., Teng, Z.H., Cao, X.D., and Zhang, J.Y., 2007b, Late Palaeozoic post-collisional magmatism in the southwestern Tianshan orogenic belt; take the Baileigong pluton in the Kokshal region as an example: Acta Petrologica Sinica, v. 23, p. 1830–1840.
- Wang, T., Hong, D.W., Tong, Y., Han, B.F., and Shi, Y.R., 2005, Zircon U-Pb SHRIMP age and origin of post-orogenic Lamazhao granitic pluton from Altai orogen: Its implications for vertical continental growth: Acta Petrologica Sinica, v. 21, p. 640–650.
- Whalen, J.B., Currie, K.L., and Chappell, B.W., 1987, A-type granites: Geochemical characteristics, discrimination and petrogenesis: Contributions to Mineralogy and Petrology, v. 95, p. 407–419, doi: 10.1007/BF00402202.
- Williams, L.S., 1998, U-Th-Pb geochronology by ion microprobe: Reviews on Economic Geology, v. 7, p. 1–35.
- Xia, L.Q., Xu, X.Y., and Xia, Z.C., 2004, Petrogenesis of Carboniferous rift-related volcanic rocks in the Tianshan, northwestern China: Geological Society of America Bulletin, v. 116, p. 419–433, doi: 10.1130/B25243.1.
- Xinjiang Bureau of Geology and Mineral Resources (B.G.M.R.), 1993, Regional Geology of the Xinjiang Uygur Autonomous Region: Beijing, Geological Publishing House, p. 17–45 (in Chinese).
- Xinjiang Bureau of Geology and Mineral Resources (B.G.M.R.), 1999, Stratigraphy of Xinjiang Uygur Autonomous Region: Beijing, China University of Geosciences Press, p. 2–19 (in Chinese).
- Xu, Y.G., Chung, S.L., Jahn, B.M., and Wu, G.Y., 2001, Petrological and geochemical constraints on the petrogenesis of the Permo-Triassic Emeishan flood basalts in southwestern China: Lithos, v. 58, p. 145–168, doi: 10.1016/S0024-4937(01)00055-X.
- Xu, Y.G., Luo, Z.Y., Huang, X.L., He, B., Xiao, L., Xie, L.W., and Shi, Y.R., 2008, Zircon U-Pb and Hf isotope constraints on crustal melting associated with the Emeishan mantle plume: Geochimica et Cosmochimica Acta, v. 72, p. 3084–3104, doi: 10.1016/j.gca.2008.04.019.
- Yang, F.Q., and Wang, L.B., 2001, Geochemistry and metallogenesis of Huoshibulake alkali-feldspar granite, Xinjiang: Geology and Resources, v. 10, p. 199–203.
- Yang, S.F., Chen, H.L., and Dong, C.W., 1995, The discovery of the Permian syenite inside of Tarim Basin and its geodynamic significance: Geochimica, v. 25, p. 121–128.
- Yang, S., Li, Z., Chen, H., Santosh, M., Dong, C., and Yu, X., 2007, Permian bimodal dyke of Tarim Basin; NW China: Geochemical characteristics and tectonic implications: Gondwana Research, v. 12, p. 113–120, doi: 10.1016/j.gr.2007.10.018.
- Yarmolyuk, V.V., and Kozlovsky, A.M., 2009, Late Carboniferous–Early Permian large igneous provinces in the Central Asian fold belt, in Abstracts of the International Symposium (6–9 August 2009): Novosibirsk, Sibprint, p. 395–398.
- Yuan, C., Sun, M., Xiao, W.J., Li, X.H., Chen, H.L., Lin, S.F., Xia, X.P., and Long, X.P., 2007, Accretionary orogenesis of the Chinese Altai: Insights from Paleozoic granitoids: Chemical Geology, v. 242, p. 22–39, doi: 10.1016/j.chemgeo.2007.02.013.
- Zhang, C.L., Li, X.H., Li, Z.X., Ye, H.M., and Li, C.N., 2008, A Permian layered intrusive complex in the western Tarim block, northwestern China: Product of a ca. 275 Ma mantle plume?: The Journal of Geology, v. 116, p. 269–287, doi: 10.1086/587726.
- Zhang, L.F., Ai, Y.L., Li, X.P., Rubatto, D., Song, B., Williams, S., Song, S.G., Ellis, D., and Liu, J.G., 2007, Triassic collision in western Tianshan orogenic belt, China: Evidence from SHRIMP U-Pb dating of zircon from HP/UHP eclogitic rocks: Lithos, v. 96, p. 266–280, doi: 10.1016/j.lithos.2006.09.012.

- Zhang, X.H., Zhang, H.F., Tang, Y.J., Simon, A.W., and Hu, Z.C., 2008, Geochemistry of Permian bimodal volcanic rocks from central Inner Mongolia, North China: Implication for tectonic setting and Phanerozoic continental growth in Central Asian orogenic belt: *Chemical Geology*, v. 249, p. 262–281, doi: 10.1016/j.chemgeo.2008.01.005.
- Zhao, Z.H., Bai, Z.H., Xiong, X.L., Mei, H.J., and Wang, Y.X., 2003, $^{40}\text{Ar}/^{39}\text{Ar}$ chronological study of late Paleozoic volcanic-hypabyssal igneous rocks in Western Tianshan, Xinjiang: *Geochimica*, v. 32, p. 317–327.
- Zhao, Z.H., Guo, Z.J., Han, B.G., Wang, Y., and Liu, C., 2006, Comparative study on Permian basalts from eastern Xinjiang-Beishan area of Gansu Province and its tectonic implications: *Acta Geologica Sinica*, v. 22, p. 1279–1293.
- Zhao, Z.H., Xiong, X.L., Wang, Q., Bai, Z.H., and Qiao, Y.L., 2007, Underplating during late Paleozoic in North Xinjiang—Evidence from shoshonitic series volcanic rocks and adakite: *Acta Geologica Sinica*, v. 81, p. 606–619.
- Zheng, C.Q., Xu, X.C., Takenori, K., and Masaki, E., 2007, Permian CHIME ages of monazites from the kyanite-sillimanite type metamorphic belt in Chonghuier area, Altai, Xinjiang and their geological implications: *Geological Journal of China Universities*, v. 13, p. 566–573.
- Zhong, S., Zhang, N., Li, Z.X., and Roberts, J.H., 2007, Supercontinent cycles, true polar wander, and very long-wavelength mantle convection: *Earth and Planetary Science Letters*, v. 261, p. 551–564, doi: 10.1016/j.epsl.2007.07.049.
- Zhou, D.W., Liu, Y.Q., Xin, X.J., Hao, J.R., Dong, Y.P., and Ouyang, Z.J., 2006, Tracing and reconstruction of the palaeo-tectonic background of the Permian basalts in Tuha and Sangtanghu Basins, NW China: *Science in China*, v. 26, p. 143–153.
- Zhou, G., Zhang, Z.C., Luo, S.B., Li, J.G., He, B., and Zhang, X.L., 2006, Zircon SHRIMP U-Pb age and biotite ^{40}Ar - ^{39}Ar age of the gneiss granite in the Mayinebo fault zone and its tectonic implications: *Acta Geologica Sinica*, v. 81, p. 359–369.
- Zhou, G., Wu, X.G., Dong, L.H., and Zhang, Z.C., 2009, Formation time and geochemical feature of the Wutubulak pluton in the northeastern margin of Junggar in Xinjiang and its geological significance: *Acta Geologica Sinica*, v. 25, p. 1930–1402.
- Zhou, M.F., Leshner, C.M., Yang, Z.X., Li, J.W., and Sun, M., 2004, Geochemistry and petrogenesis of 270 Ma Ni–Cu–(PGE) sulfide-bearing mafic intrusions in the Huangshan district, eastern Xinjiang, northwest China: Implications for the tectonic evolution of the Central Asian orogenic belt: *Chemical Geology*, v. 209, p. 233–257, doi: 10.1016/j.chemgeo.2004.05.005.
- Zokh, A.E., Polyakov, G.V., Vishnevsky, A.V., Shelepaev, R.A., and Oyunchimeg, T., 2009, Age of ultramafic magmatism in western Mongolia, in *Large Igneous Provinces of Asia; Mantle Plumes and Metallogeny: Abstracts of the International Symposium (6–9 August 2009)*: Novosibirsk, Sibprint, p. 137–140.

MANUSCRIPT RECEIVED 9 JANUARY 2009
 REVISED MANUSCRIPT RECEIVED 17 OCTOBER 2009
 MANUSCRIPT ACCEPTED 20 OCTOBER 2009

Printed in the USA